



HAL
open science

Lateral Variations in Foreland Flexure of a Rifted Continental Margin: The Aquitaine Basin (SW France)

P. Angrand, M. Ford, A. B. Watts

► **To cite this version:**

P. Angrand, M. Ford, A. B. Watts. Lateral Variations in Foreland Flexure of a Rifted Continental Margin: The Aquitaine Basin (SW France). *Tectonics*, 2018, 37 (2), pp.430-449. 10.1002/2017TC004670 . insu-03712923

HAL Id: insu-03712923

<https://insu.hal.science/insu-03712923>

Submitted on 4 Jul 2022

HAL is a multi-disciplinary open access archive for the deposit and dissemination of scientific research documents, whether they are published or not. The documents may come from teaching and research institutions in France or abroad, or from public or private research centers.

L'archive ouverte pluridisciplinaire **HAL**, est destinée au dépôt et à la diffusion de documents scientifiques de niveau recherche, publiés ou non, émanant des établissements d'enseignement et de recherche français ou étrangers, des laboratoires publics ou privés.

Copyright



RESEARCH ARTICLE

10.1002/2017TC004670

Key Points:

- Inherited rifting can control the evolution of a foreland basin that develops before the thinned lithosphere has thermally equilibrated
- Rift intensity below the Aquitaine Basin increases west correlating with decreasing flexural strength and increasing postrift subsidence
- Subsidence in the Aquitaine foreland basin combines flexural loading (surface and subsurface) and postrift thermal cooling

Correspondence to:

P. Angrand,
pangrand@crpg.cnrs-nancy.fr

Citation:

Angrand, P., Ford, M., & Watts, A. B. (2018). Lateral variations in foreland flexure of a rifted continental margin: The Aquitaine Basin (SW France). *Tectonics*, 37, 430–449. <https://doi.org/10.1002/2017TC004670>

Received 19 MAY 2017

Accepted 9 JAN 2018

Accepted article online 15 JAN 2018

Published online 7 FEB 2018

Lateral Variations in Foreland Flexure of a Rifted Continental Margin: The Aquitaine Basin (SW France)

P. Angrand¹ , M. Ford¹ , and A. B. Watts² 

¹CRPG, UMR 7358, Nancy, France, ²Department of Earth Sciences, University of Oxford, Oxford, UK

Abstract Rift inheritance can play a key role in foreland basin geometry and behavior. If the foreland basin initiates soon after rifting, thermal cooling can also contribute significantly to subsidence. We investigate the effects of crustal inheritance (Aptian-Cenomanian rifting) on the evolution of the Campanian to middle Miocene flexural Aquitaine foreland basin, northern Pyrenees, France. Surface and subsurface data define rifted crustal geometry and postrift thermal subsidence. Analysis of Bouguer gravity anomalies coupled with flexural modeling constrains the lateral variations of elastic thickness, plate flexure, and controlling loads. The Aquitaine foreland is divided along-strike into three sectors. The relative role of surface and subsurface (i.e., buried) loading varies along-strike, and the elastic thickness values decrease from the northeast (25 km) to the southwest (7 km) where the plate is the most stretched. The eastern foreland crust was not rifted and underwent a simple flexural subsidence in response to orogenesis. The central sector was affected by crustal stretching. Here the basin is modeled by combining topographic and buried loads, with postrift thermal subsidence. In the western sector, the foreland basin was created mainly by postrift thermal subsidence. The eastern and central sectors are separated by the Eastern Crustal Lineament, which is one of a series of inherited transverse faults that segment the orogen.

1. Introduction

Peripheral foreland basins form by lithospheric flexure in front of migrating orogenic loads (e.g., Beaumont, 1981; Dickinson, 1974; Garcia-Castellanos et al., 2002; Gaspar-Escribano et al., 2001; Haddad & Watts, 1999; Horton & DeCelles, 1997; Ingersoll, 1988; Lyon-Caen & Molnar, 1983, 1985; Stewart & Watts, 1997). Flexural studies indicate that foreland basin geometry primarily depends on the surface (i.e., topographic) loads of a growing orogen and the flexural rigidity of the lithosphere, often expressed as its effective elastic thickness (T_e) (Burov & Diament, 1995; DeCelles, 2012; Karner & Watts, 1983; Molnar & Lyon-Caen, 1988; Turcotte & Schubert, 2002; Watts, 2001). Lithospheric flexure can also be enhanced by other processes such as slab pull, intraplate stress, and the presence of dense bodies at depth (Ford et al., 2006; Lyon-Caen & Molnar, 1983, 1985; Royden & Karner, 1984; Watts, 2001). For example, buried loads have been successfully invoked to explain the discrepancy between calculated flexure due to surface topography and observed flexure in Taiwan (Lin & Watts, 2002) and the United Arab Emirates (Ali & Watts, 2009).

Many foreland basins are superimposed on ancient rift systems, which may also have a fundamental influence on their evolution (e.g., DeCelles et al., 2011; Desegaulx et al., 1991; Horton et al., 2016; Watts, 1992; Willett et al., 1984). While several studies suggest that inherited rift structures may weaken the lithosphere and thus reduce T_e (e.g., Papua New-Guinea, Haddad & Watts, 1999; Taiwan, Lin & Watts, 2002; Southern Andes, Fosdick et al., 2014), a detailed study of this topic is lacking. In addition, depending on the thermal age of the rifted lithosphere at the onset of convergence, a component of postrift thermal subsidence may actively contribute to foreland subsidence (e.g., Desegaulx et al., 1991).

In this paper we investigate the flexural geometry and behavior of the Aquitaine foreland basin, SW France, which developed on a relatively young and complex rifted crust. The Aquitaine Basin is the Pyrenean retroforeland basin (Naylor & Sinclair, 2008) that developed on the upper (European) plate from Campanian to middle Miocene (Puigdefàbregas & Souquet, 1986; Figures 1b and 1d). The present-day topography of the Pyrenees is insufficient to fully explain the observed flexure of either the pro-foreland basin (Gaspar-Escribano et al., 2001) or the retro-foreland basin (Desegaulx et al., 1991). Therefore, additional subsidence driving mechanisms are required. The geology of the Aquitaine Basin has been widely studied for hydrocarbons exploration (BRGM et al., 1974; Biteau et al., 2006; Serrano et al., 2006). Previous work has shown that part of the synorogenic basin developed above inherited rift depocenters (Biteau et al., 2006; Brunet, 1994;

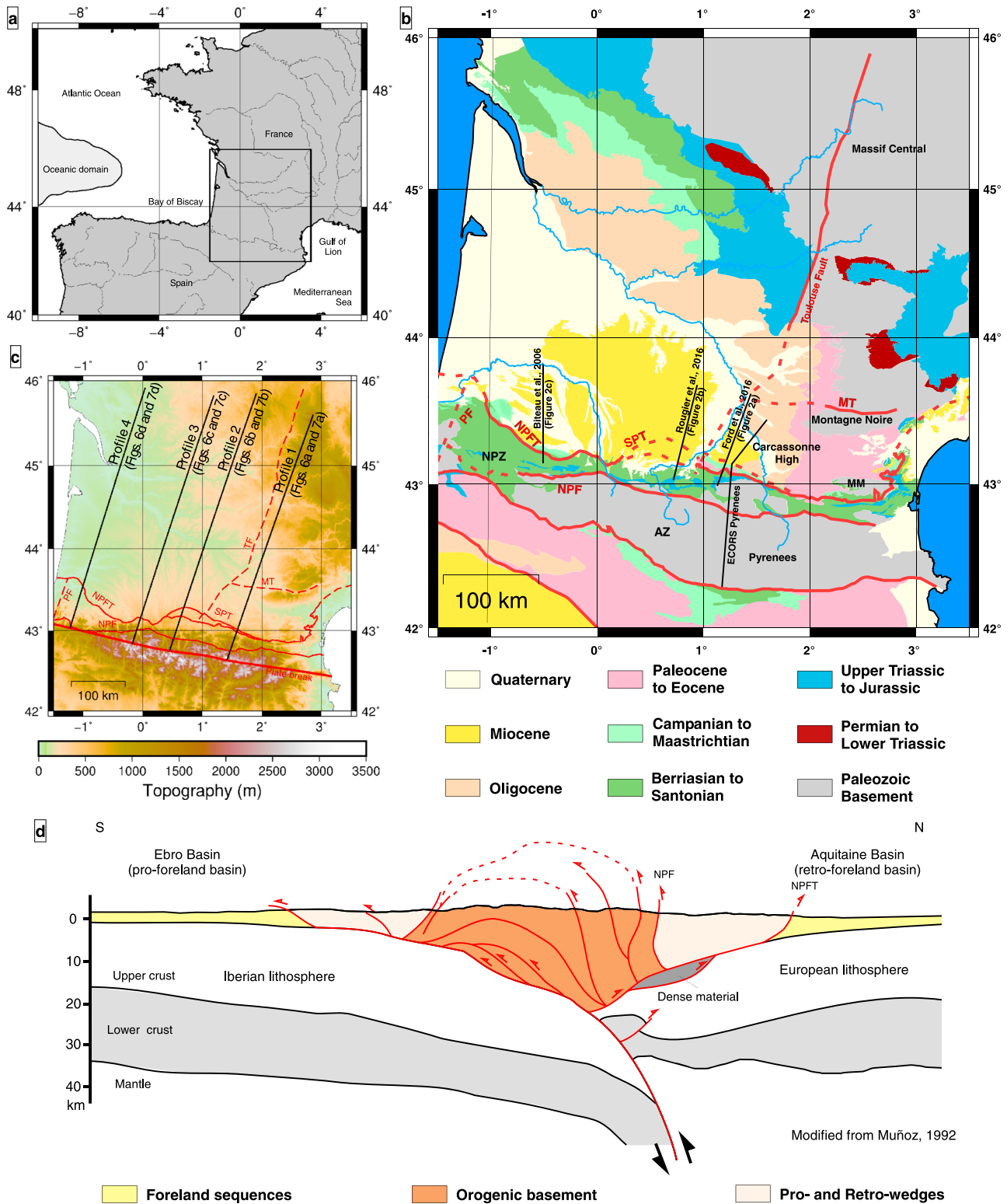


Figure 1. Location map, geological map, and topographic map of the study area and a simplified crustal model for the Pyrenean orogen. AZ: Axial Zone; NPZ: North Pyrenean Zone; NPF: North Pyrenean Fault; NPFT: North Pyrenean Frontal Thrust; SPT: Sub-Pyrenean Thrust; PF: Pamplona Fault; MT: Mazamet Thrust; MM: Mouthoumet Massif. (a) Location map of the study area. Note the occurrence of the domain of oceanic crust west of the Aquitaine Basin (contour from Tugend et al., 2015). The black contour represents the location of Figures 1b and 1c. (b) Simplified geological map of the Aquitaine Basin, showing the location of cross sections in Figures 1d and 2. (c) Topographic map of the study area. See locations of the flexural profiles of Figures 6 and 7. (d) Simplified crustal model along the ECORS Pyrenees deep seismic profile (modified from Muñoz, 1992). See location on Figure 1b.

Canérot et al., 2005; Serrano et al., 2006) and suggests that the western basin records a component of postrift thermal subsidence (Desegaulx et al., 1991).

In our analysis, we address the following questions: What was the effect of thinned lithosphere on the evolution of the Aquitaine foreland basin? Can we distinguish postrift thermal subsidence from orogenic load-induced flexural subsidence? What were the sources of loading that caused flexure of the European plate? Is the crust underneath the foreland segmented and did this affect basin evolution? We address these questions by (1) using surface and subsurface data to define the present-day geometry of the foreland basin, the depth to Paleozoic basement, and Moho depth and thus derive crustal thickness; (2) using these data to estimate crustal stretching and thus derive the amount of postrift thermal subsidence that occurred during orogenesis; (3) analysis of Bouguer gravity anomaly data coupled with flexural modeling to constrain the lateral variations in elastic thickness, plate flexure, and the contribution of both surface and subsurface loads. We can thus compare and quantify the variable roles of an inherited rifted crust and of surface and subsurface loads in controlling foreland basin geometry. We show that flexure due to topographic loading alone cannot explain the observed foreland basin succession and that postrift thermal subsidence is locally an important component of subsidence of the Aquitaine Basin as it developed only 10 Myr after the end of Aptian-Cenomanian rifting.

2. Geological Setting

2.1. Structure

The Pyrenean mountain chain is a 110°N trending Alpine orogen created by convergence and collision of the Iberian and European plates, from early Campanian to middle Miocene (Beaumont et al., 2000; Choukroune & ECORS Pyrenees Team, 1989; Christophoul et al., 2003; Choukroune et al., 1990; Fitzgerald et al., 1999; Puigdefàbregas & Souquet, 1986; Roure et al., 1989; Sinclair et al., 2005; Vergés et al., 1995; Figures 1b and 1d and 2d). The double-wedge orogen is ~400 km long, ~100 km wide and consists of a prowedge on the Iberian plate to the south and a retro-wedge on the upper European plate (Figure 1d). The crustal root of the belt reaches a depth of ~50 km due to northward subduction of the Iberian lower crust and lithospheric mantle (Choukroune & ECORS Pyrenees Team, 1989; Choukroune et al., 1990; Chevrot et al., 2014; Daignières et al., 1981). Estimates of N-S shortening in the eastern Pyrenees range from 100 to 165 km (Beaumont et al., 2000, 165 km; Choukroune & ECORS Pyrenees Team, 1989; Choukroune et al., 1990, 100 km; Mouthereau et al., 2014, 142 km; Muñoz, 1992, 147 km). In the western part of the chain Teixell (1998) proposes 75–80 km of shortening. The highest topography reaches ~3,300 m above sea level (Figure 1c).

The north Pyrenees consist of three tectonostratigraphic units (from south to north) (Figures 1b and 2a and 2b): the North Pyrenean Zone (NPZ), the Sub-Pyrenean Zone (SPZ) in the center and eastern retrowedge, and the Aquitaine foreland basin. To the south, the Axial Zone (AZ) comprises south-verging imbricates of Paleozoic rocks. The NPZ is a narrow (15–30 km) thick-skinned fold-thrust belt comprising nonmetamorphic Mesozoic sedimentary rocks and Paleozoic basement massifs to the north and a zone of LP-HT (up to 600°C) metamorphism of Albo-Cenomanian age, associated with breccia and peridotite bodies (Albarède & Michard-Vitrac, 1978; Fabriès et al., 1998; Golberg & Leyreloup, 1990; Henry et al., 1998; Vielzeuf & Kornprobst, 1984) to the south. These features are widely interpreted to represent remnants of an inverted hyper-thinned Aptian-Cenomanian rift system (e.g., Jammes et al., 2009; Lagabrielle & Bodinier, 2008). Major boundary faults are the North Pyrenean Fault (NPF) between the AZ and NPZ, the North Pyrenean Pyrenean Thrust (NPFT) to the north of the NPZ, and the Sub-Pyrenean Thrust (SPT) between the SPZ and the Aquitaine Basin (Figures 1b and 2a and 2b). The NPF is an inherited crustal fault with strike-slip kinematics and is generally assumed to be the surface expression of the boundary between Iberian and European crusts (Choukroune & Mattauer, 1978).

2.2. Tectonic Evolution

A first rifting event took place during Permian to Lower Triassic, associated with breakup of Pangea (Olsen, 1997). A second, major rifting event (Aptian-late Cenomanian) generated the westward opening V-shaped Bay of Biscay oceanic basin (e.g., Olivet, 1996; Sibuet et al., 2004; Figure 1a), while extreme crustal thinning associated with exhumation of lithospheric mantle and lower crust, and high temperature metamorphism occurred further east where no oceanic crust was created (e.g., Fabriès et al., 1998; Henry et al., 1998; Jammes et al., 2009; Lagabrielle & Bodinier, 2008; Vielzeuf & Kornprobst, 1984). Turonian-Santonian strata record thermal cooling of the previously rifted lithosphere. The onset of convergence started at ~84 Ma

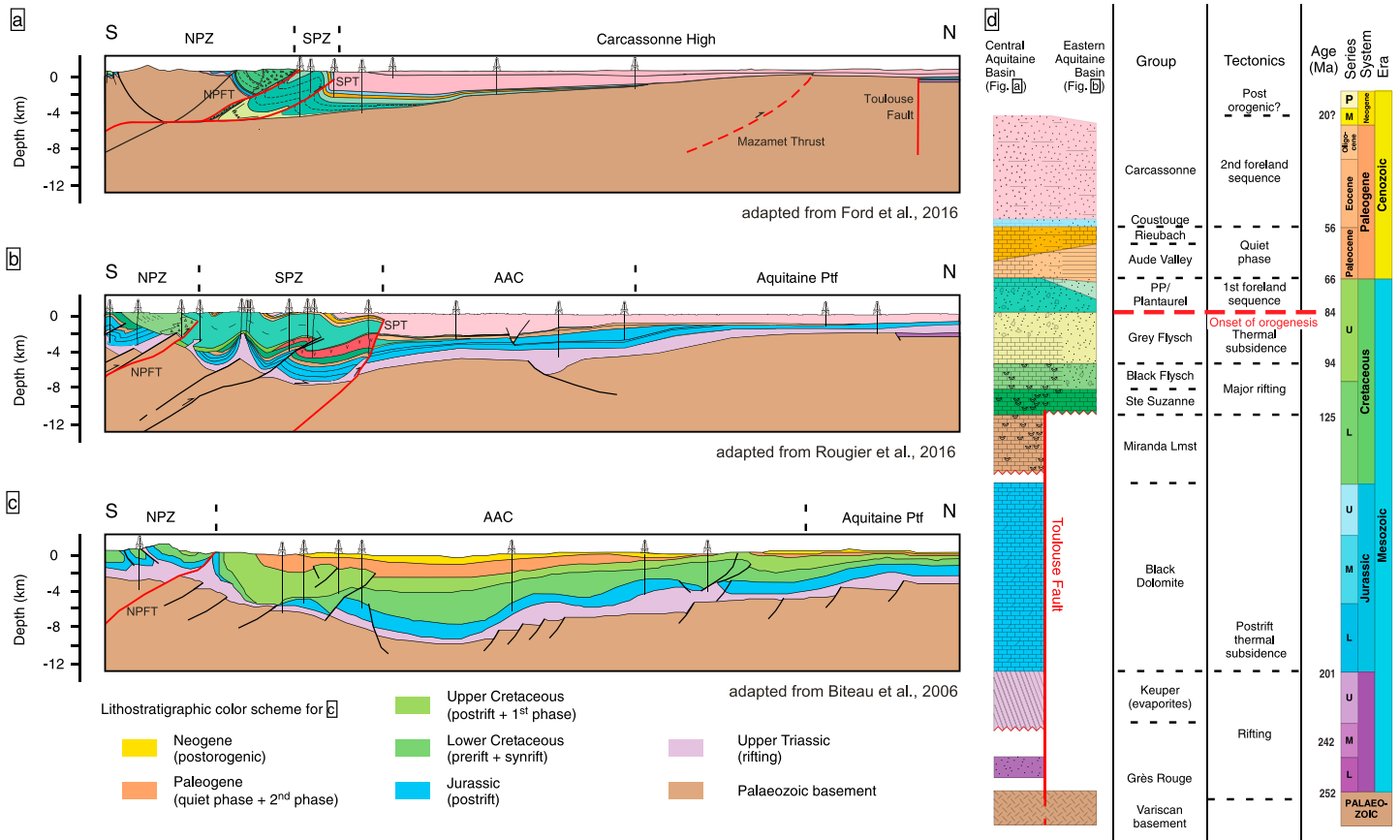


Figure 2. Structural cross sections, stratigraphy, and tectonic history summary for the central and eastern Aquitaine Basin. NPFT: North Pyrenean Frontal Thrust; SPT: Sub-Pyrenean Thrust; AZ: Axial Zone of the Pyrenees; NPZ: North Pyrenean Zone; SPZ: South Pyrenean Zone; AAC: Adour-Arzacq-Comminges rift; Pft: platform. The cross sections are located on Figure 1b. (a) Cross section through the eastern Aquitaine Basin (adapted from Ford et al., 2016). The colors used are those in the stratigraphic chart in Figure 2d. (b) Cross section through the central Aquitaine Basin (adapted from Rougier et al. (2016)). The colors used are those in the stratigraphic chart in Figure 2d. (c) Cross section through the western Aquitaine Basin (adapted from Biteau et al. (2006)). Note that this cross section has a distinct lithostratigraphic color scheme. (d) Stratigraphic chart and major tectonic events, compiled from Ford et al. (2016) and Rougier et al. (2016) for the eastern and central Aquitaine Basin.

(e.g., Ford et al., 2016; Mouthereau et al., 2014; Rahl et al., 2011; Rougier et al., 2016). Therefore, the time gap between the end of rifting and the onset of orogeny is only 10 Myr (Figure 2d). As no oceanic crust was generated (Chevrot et al., 2014; Mouthereau et al., 2014) continental collision did not involve oceanic plate subduction. The Pyrenean orogeny has two phases. The first phase (Campano-Maastrichtian) involves closure of the exhumed mantle domain accompanied by distributed inversion of rift structures and a first subsidence phase in the foreland basins (Desegaux & Brunet, 1990; Ford et al., 2016; Rougier et al., 2016). The second phase (Eocene to middle Miocene) of full continental collision is also well recorded in the foreland basins. These two phases are separated by a Paleocene quiet phase (Ford et al., 2016; Mouthereau et al., 2014; Sinclair et al., 2005).

2.3. Stratigraphy

Permo-Triassic rifting is recorded in the NPZ by nonmarine sedimentation (Grès Rouge Formation; Lucas, 1985), followed by the dolomite to evaporite succession in the Upper Triassic (BRGM et al., 1974; Curnelle, 1983). Marine Jurassic to Early Cretaceous (Berriasian-Barremian) carbonate series were deposited in a platform setting west of the Toulouse Fault (Figures 2b–2d). The Upper Jurassic/Early Cretaceous boundary is marked by the erosive Cimmerian unconformity in the southernmost part of the Aquitaine Basin and in the NPZ (Canérot et al., 2005; James & Canérot, 1999). Locally thickness variations of Jurassic and lower Cretaceous series are due to salt tectonics (Figures 2b and 2c; Biteau et al., 2006; Canérot et al., 2005; Rougier et al., 2016). The second rift phase is recorded in the Aptian-Cenomanian carbonate platforms

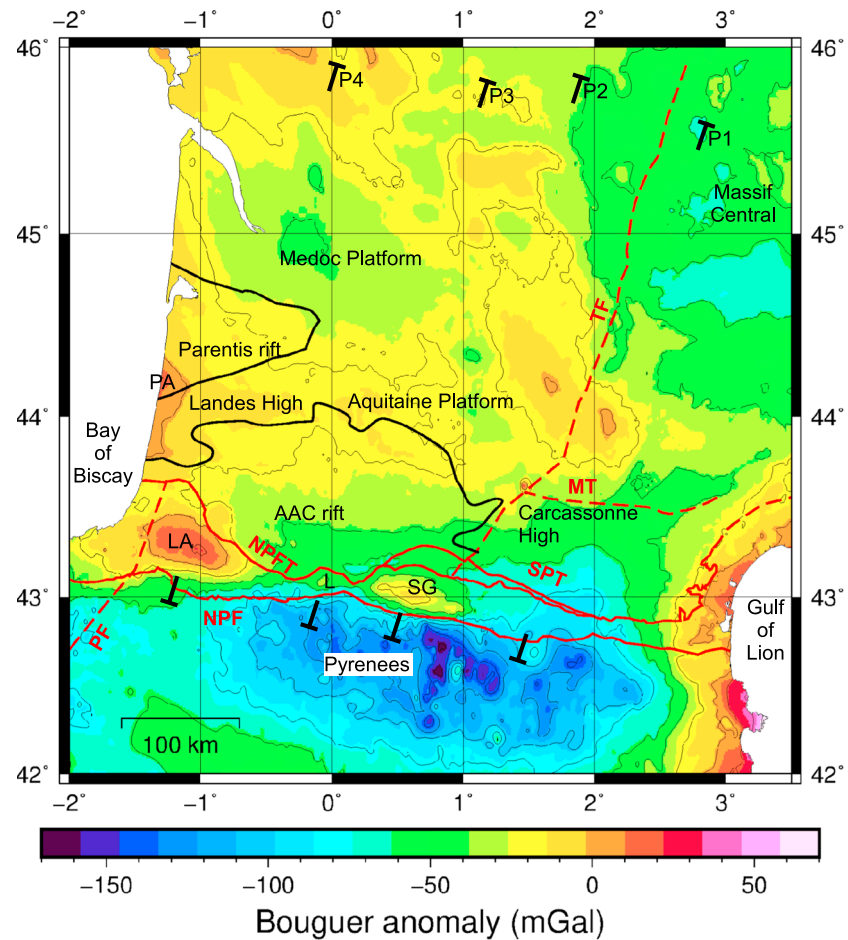


Figure 3. Map of Bouguer anomaly values across the Pyrenees, SW France. These data are provided by the International Gravimetric Bureau (BGI, 2012). The contours are every 20 mGal. Major positive anomalies are as follows: PA: Parentis; LA: Labourde; L: Lourdes; SG: Saint-Gaudens. The black rectangle shows the location of Figures 4 and 5. Profiles P1 to P4 are presented in Figures 6 and 7. Superimposed major structures (red) are as follows: NPF: North Pyrenean Fault; NPFT: North Pyrenean Frontal Thrust; SPT: Sub-Pyrenean Thrust; TF: Toulouse Fault; PF: Pamplona Fault; MT: Mazamet Thrust. Major Aptian-Cenomanian depocenters are outlined in black (Parentis and Adour-Arzacq-Comminges (AAC) rift-basins).

fringing a series of deep depocenters infilled with turbidites (Sainte Suzanne and Black Flysch Groups; Debroas, 1990; Souquet et al., 1985). Turonian-Santonian turbidites were then deposited during the thermal cooling phase. The Aquitaine Basin preserves a Campanian-middle Miocene synorogenic sedimentary series up to 5.5 km thick (Figures 2 and 4). The stratigraphic succession shows a consistent facies change from predominantly nonmarine in the east to predominantly marine to the west (BRGM et al., 1974). In the central basin, Campanian-Maastrichtian marine turbidites (Petites Pyrenees Group) pass eastward into deltaic and then fluvial sandstones (Plantaurel Group). Overlying Paleocene marine (Rieubach Group) to nonmarine detrital and carbonate facies (Aude Valley Group) are followed everywhere by the marine facies of the Coustouge Group. The uppermost fluvial and lacustrine Carcassonne Group (Eocene-middle Miocene) in the east and center was sourced from the uplifting orogen to the south with equivalent to marine facies in the west (Figure 2d; BRGM et al., 1974; Christophoul et al., 2003; Ford et al., 2016; Rougier et al., 2016).

3. Bouguer Gravity Anomalies

Following similar studies in other orogenic belts, we here use gravity anomalies to investigate the flexure of the European lithosphere and the geometry and density of the controlling loads (i.e., surface or buried) (Casas

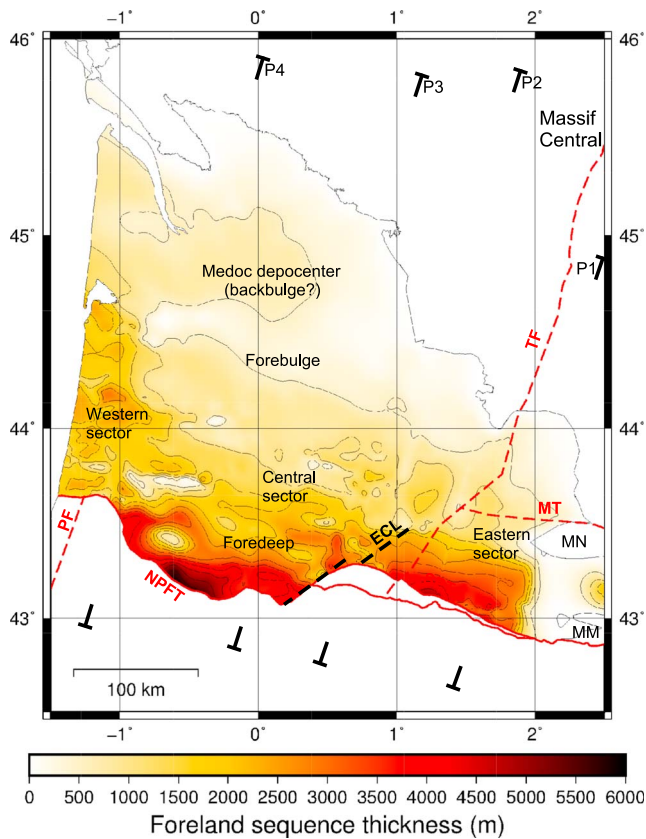


Figure 4. Thickness map of the synorogenic foreland basin succession of the Aquitaine Basin (Campanian–middle Miocene), derived from a compilation of data from structural cross sections (PYRAMID cross sections: Ford et al., 2016; Rougier et al., 2016; and other ongoing works) and isopach maps (BRGM et al., 1974). The white areas to the north have no foreland basin succession. The white areas to the south of the NPFT represent the orogen. The contours are every 500 m. Profiles P1 to P4 are presented in Figures 6 and 7. NPFT: North Pyrenean Frontal Thrust; SPT: Sub-Pyrenean Thrust; TF: Toulouse Fault; PF: Pamplona Fault; ECL: Eastern Crustal Lineament; MN: Montagne Noire; MT: Mazamet Thrust; MM: Mouthoumet Massif.

emplaced northward into the crust during the Pyrenean orogenesis (Casas et al., 1997; de Cabissole, 1990; Jammes, Lavier, et al., 2010; Muñoz, 1992; Pedreira et al., 2003, 2007; Torné et al., 1989). Pedreira et al. (2003) propose that the Labourd anomaly results from a large mantle body that was exhumed during Early Cretaceous extension and subsequently thrust into the upper European crust during Pyrenean inversion. This mode of emplacement could also be valid for the Lourdes and Saint-Gaudens anomalies. Alternatively, Velasque et al. (1989) propose that the Labourd anomaly is caused by a mantle uplift model (to 15 km depth). This model has recently been supported by seismic tomographic imaging data (Wang et al., 2016). These hypotheses will be considered using 2-D flexural modeling along sections that cross these positive gravity anomalies.

4. Aquitaine Basin Geometry

Figure 4 presents a new map of the total preserved thickness of the foreland basin succession derived from a compilation of published isopach maps and both published and unpublished structural cross sections (BRGM et al., 1974; Ford et al., 2016; Rougier et al., 2016). Three sectors (east, central, and west, Figure 4) are recognized in the basin based on along-strike variations in basin geometry, sediment thickness, distribution, and deformation (described below). Overall, the basin succession thickens southward, with the greatest thickness in the central sector. We delimit the eastern and central sectors by a broad NE-SW lineament that also affects

et al., 1997; Contreras-Reyes & Osses, 2010; Karner & Watts, 1983; Lin & Watts, 2002; Molnar & Lyon-Caen, 1988).

The Bouguer anomaly map of the central Pyrenees and its northern foreland (Figure 3) corresponds to that of a typical orogen (Daignières et al., 1994; Karner & Watts, 1983). It is characterized by (a) a large negative anomaly (to -170 mGal) over the AZ related to the orogen's crustal root, (b) a weak negative anomaly over the central foredeep due to its sedimentary infill and flexure of the crust, and (c) a weak positive anomaly over the Aquitaine Platform representing the forebulge (e.g., Ali et al., 2014; Daignières et al., 1994). Relatively low Bouguer anomalies in the northeast and east of the map area correspond to the Massif Central (Figure 1b).

In the onshore western sector, however, the gravity anomalies do not present a pattern typical of a flexural foreland basin. Along the Atlantic coastline, the south Parentis area is characterized by a large positive Bouguer anomaly (PA; Figure 3) that continues westward offshore where the authors propose it lies above exhumed mantle emplaced by Aptian-Cenomanian rifting (Figure 5c; Bois & ECORS Scientific Party, 1990; Jammes, Lavier, et al., 2010; Masini et al., 2014).

The AZ negative anomaly, which decreases in intensity toward the western and eastern edges of the Pyrenean range, is attributed to the thickened low density crustal root of the orogen (Daignières et al., 1982, 1989; ECORS Pyrenees Team, 1988; Torné et al., 1989). In the central sector the NPF delimits the northern edge of this negative anomaly confirming this fault as a major crustal boundary. However, in the eastern sector, the negative anomaly continues north of the NPFT, below the Carcassonne High (Figure 3), an area unaffected by Aptian-Cenomanian rifting. Farther east toward the Mediterranean Sea, late Cenozoic uplift of the rift shoulder of the Gulf of Lion passive margin is responsible for relatively high Bouguer anomalies, as the Moho shallows to ~ 22 km depth (Daignières et al., 1982; Gallart et al., 2001).

In the NPZ a series of relatively high positive Bouguer anomalies are aligned parallel to the NPFT (Saint-Gaudens, Lourdes, Labourd; SG, L, and LA, respectively; Figure 3). These anomalies have been interpreted as due to imbricates of dense material (either lower crust or mantle)

the thrust front (ECL: Eastern Crustal Lineament, Figure 4) and that is subparallel to the well-known Toulouse (Figure 1b). The ECL has no surface expression, as it is covered by recent sediments.

A full preorogenic Mesozoic series (Triassic-Santonian) is preserved west of the Toulouse Fault, while to the east this series is absent (Carcassonne High; Figures 2a and 2b). The western and central sectors of the foreland basin are characterized by a variably rifted crust and a Mesozoic succession that thickens westward (Figures 2b and 2c). This succession comprises Upper Triassic evaporites at its base (Biteau et al., 2006; BRGM et al., 1974; Canérot et al., 2005; James & Canérot, 1999; Jammes, Manatschal, et al., 2010; Serrano et al., 2006). However, as will be described below, the western sector records a distinct subsidence and deformation behavior with respect to the central foreland basin.

4.1. Eastern Basin

East of the ECL, the foreland basin succession onlaps northward directly onto nonrifted Paleozoic basement (Figure 2a). The proximal foreland basin shows a relatively simple flexural geometry, thickening to up to 5.5 km toward the south (Figure 4). North of the NPFT, the amount of shortening is low, mainly localized along the SPT (Figure 2a) in the west and on basement-involved thrusts in the east, which were active during foreland basin development. The resulting broad basement uplifts limited subsidence in the easternmost basin (e.g., Mouthoumet Massif, Figure 4). Farther north, the Mazamet Thrust defines the northern limit of the Montagne Noire Variscan massif and records Eocene-Oligocene northward thrusting (Figure 1b; Demange & Jamet, 1986). We do not recognize any changes in the thickness or geometry of the foreland succession across the trace of the Toulouse Fault. However, there is clearly a major southward shift in the position of the basin depocenter across the ECL (Figure 4).

Only the southern part of the eastern foreland basin is preserved east of the Toulouse Fault. Post-Oligocene uplift of the Massif Central (Michon & Merle, 2001) and rift shoulder uplift linked to crustal extension and formation of the Gulf of Lion in the Oligo-Miocene (e.g., Gunnell et al., 2008; Mauffret et al., 2001; Seranne, 1999) led to major erosion of the northern and eastern foreland basin (Figure 1b). Because of this, a full analysis of the flexural behavior of the eastern basin was not possible.

4.2. Central Basin

In the central sector the basin broadens to a maximum N-S width of ~300 km (Figure 4). The NPFT steps south by ~45 km (as does the foredeep) with respect to its position to the east and west. While showing an overall southward thickening to 5.5 km, the foredeep also displays complex thickness variations due to local thrust and salt tectonics (Figure 2b; Canérot et al., 2005; James & Canérot, 1999; Rougier et al., 2016). Shortening in the SPZ is accommodated by local and short-scale tectonic inversions of salt-rich extensional structures (Rougier et al., 2016). Approximately 200 km north of the NPFT, the synorogenic succession thins (to 1 km) across a 20–50 km wide area (Aquitaine platform), which we identify as the forebulge. Farther north a second minor depocenter (Medoc depocenter; Figure 4) preserves less than 1 km of Paleocene-middle Miocene sedimentary rocks. Although its amplitude is rather high, this could be interpreted as the backbulge (Figure 4, DeCelles & Giles, 1996). Such discrepancies may arise from inherited structures, locally nonelastic mechanisms of subsidence in the backbulge, or interference with the flexural signal from the northern craton (DeCelles & Horton, 2003; Horton & DeCelles, 1997; Waschbusch & Royden, 1992).

4.3. Western Basin

Farther west along the Atlantic coastline, the thickness of the Aquitaine Basin succession does not show the characteristic asymmetrical flexural pattern (Figure 4) of a foreland basin. Instead, sediment thicknesses describe a broad depocenter thickening westward toward the Bay of Biscay (Biteau et al., 2006; Brunet, 1994; Ferrer et al., 2012; Tugend et al., 2014). Figure 2c (Biteau et al., 2006) shows that the foredeep is clearly localized above extensional structures. The western foreland also records less Pyrenean shortening (Teixell, 1998). The significance of these features will be discussed below.

5. Crustal Structure: Analysis of Inherited Rifting

5.1. Depth to Top Paleozoic Basement

Figure 5a shows the depth below sea level of the top to Paleozoic basement (stratigraphically below Upper Triassic) derived from a compilation of isobath maps (BRGM et al., 1974), structural cross sections (Ford et al.,

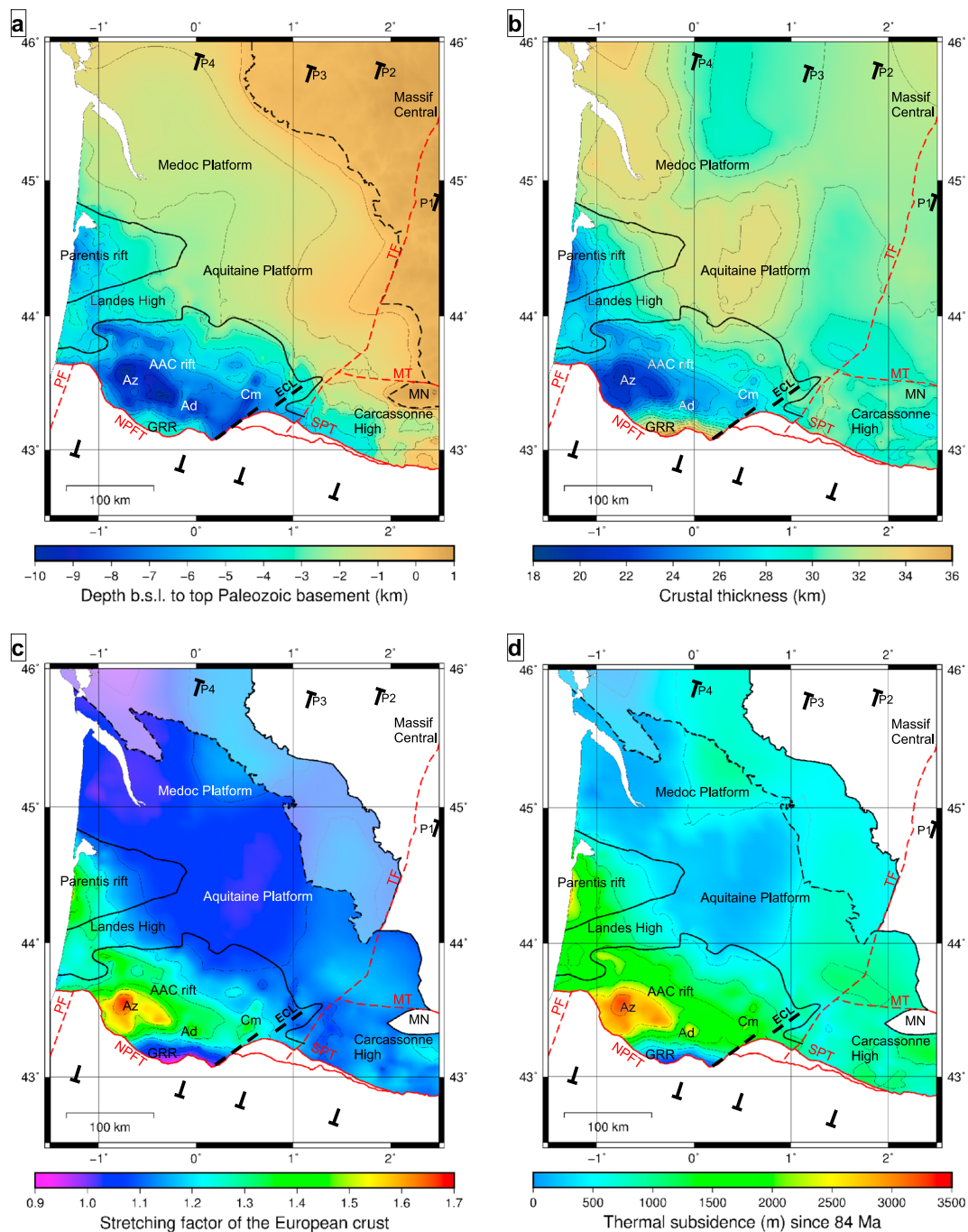


Figure 5. Analysis of crustal thinning due to rifting below the Aquitaine Basin. The white areas are deformed areas south of the NPFT and SPT. Profiles P1 to P4 are presented in Figures 6 and 7. NPFT: North Pyrenean Frontal Thrust; SPT: Sub-Pyrenean Thrust; TF: Toulouse Fault; PF: Pamplona Fault; ECL: Eastern Crustal Lineament; AAC: Arzacq-Adour-Comminges; Az: Arzacq subbasin; Ad: Adour subbasin; Cm: Comminges subbasin; GRR: Grand-Rieu Ridge; MN: Montagne Noire; MM: Mouthoumet Massif. (a) Map of depth below sea level to top Paleozoic basement in the Aquitaine Basin. Compilation of data from isobath maps (BRGM et al., 1974), structural cross sections (PYRAMID cross sections: Ford et al., 2016; Rougier et al., 2016; and other ongoing works), and interpreted seismic profiles (Serrano et al., 2006). The dashed black line represents the outcropping Paleozoic Massif Central. The contours are every 1,000 m. (b) Crustal thickness map of the European plate calculated using depth to top Paleozoic basement in Figure 5a and depth to Moho (source: Bureau des Ressources Géologiques et Minières, French Geological Survey). The contours are every 1,000 m. (c) Stretching factor map for the European crust (β). β is the ratio of the observed to an initial crustal thickness of 34 km. Note edge effects to the south of the GRR. The transparent area northeast of the bold dashed black line represents preorogenic sedimentary cover where data are affected by deformation of the massif central. The white area to the northeast represents the Paleozoic Massif Central. The contours are every 0.1. (d) Map of postrift thermal subsidence since the onset of orogenesis (S_{to}) (84 Ma). S_{to} is based on the β value (uniform stretching model, McKenzie, 1978). Note the edge effects to the south of the GRR. The transparent area northeast of the bold dashed black line represents preorogenic sedimentary cover where data are affected by deformation of the Massif Central. The white area to the northeast represents the Paleozoic Massif Central. The contours are every 500 m.

2016; Rougier et al., 2016), and interpreted seismic profiles (Serrano et al., 2006). West of the Toulouse Fault, the basement gently deepens south and southwest across the northern Medoc and Aquitaine Platforms where no rift structures are identified (stable platform of Biteau et al. (2006)).

To the south in the central sector, top basement deepens to ~10 km under the Aptian-Cenomanian Arzacq-Adour-Comminges (AAC) rift basin (Figure 5a; Biteau et al., 2006; Canérot et al., 2005; Serrano et al., 2006; Rougier et al., 2016). This deep rift basin trends WNW-ESE and has a complex form with three subbasins, the Arzacq (Az), Adour (Ad), and Comminges (Cm). It is limited to the east by the ECL. In the eastern sector, the Carcassonne High, which was not subjected to major rifting, is characterized by a shallower basement that deepens asymmetrically to the south, clearly reflecting synorogenic flexure.

In the western sector, the AAC basin terminates to the northwest against the Landes High and is locally bounded to the south by the Grand-Rieu Ridge (GRR). Both are paleogeographic highs inherited from Early Cretaceous rifting (Bourrouilh et al., 1995; Ferrer et al., 2008, 2012; Serrano et al., 2001; Teixell et al., 2016). North of the WSW-ENE trending Landes High, the Parentis rift opens westward to the oceanic domain of the Bay of Biscay (Figure 1a; Ferrer et al., 2012; Jammes, Tiberi, et al., 2010).

5.2. Crustal Thickness and Stretching of the Crust

Crustal thickness (Figure 5b) in the Pyrenean foreland has been calculated by subtracting the depth to top Paleozoic basement (Figure 5a) from depth to Moho. We use a depth to Moho from a compilation of seismic reflection and refraction data (Bureau des Ressources Géologiques et Minières, French Geological Survey). Crustal thinning below the AAC and Parentis rifts is clearly identified. The main area of Aptian-Cenomanian crustal thinning would have lain farther south and is now integrated into the NPZ (e.g., Jammes et al., 2009; Lagabrielle & Bodinier, 2008). Figure 5c shows the calculated stretching factor (β) for the European crust, derived by comparing observed crustal thickness to a mean crustal thickness reference value of 34 km, observed below the unstretched Medoc and Aquitaine Platforms (Figure 5b), cratonward of the rift domain. Although it is a first approximation, assume that after the continental rifting during Permo-Triassic times and thermal reequilibration during the Jurassic and early Cretaceous, the lithosphere of the future Aquitaine Basin was in equilibrium with a uniform crustal thickness at the onset of Aptian-Cenomanian rifting.

β increases rapidly to the south and west of the northern stable platform, with a maximum β of 1.65 in the western AAC rift (Figure 5c). To the south of the AAC the inherited Grand-Rieu Ridge records local low β with an edge effect of β values <1 along its southern boundary (NPFT). As expected, β is around 1 on the Carcassonne High to the east. To the northeast toward the Massif Central, data are extrapolated and must therefore be considered with caution.

The Parentis rift, which shows a maximum onshore β of 1.45 (Figure 5c), records hyper-extension offshore (Ferrer et al., 2012; Tugend et al., 2014). It forms the eastern limit of the northern Bay of Biscay passive margin. The oceanic domain starts ~500 km west of the Atlantic coastline (Figure 1c).

5.3. Postrift Thermal Subsidence

The major rifting between the European and Iberian plates initiated in the Aptian and ended during late Cenomanian (Clerc et al., 2012; Debroas, 1987, 1990; Jammes et al., 2009; Lagabrielle & Bodinier, 2008; Puigdefàbregas & Souquet, 1986; Tugend et al., 2015; Figure 2d). The initial (synrift) subsidence is recorded in the Aptian-Cenomanian deep marine turbidites of the Black Flysch Group in the NPZ and the southern part of the Aquitaine Basin (AAC rift; Debroas, 1987, 1990; Puigdefàbregas & Souquet, 1986; Souquet et al., 1985). Turonian-Santonian postrift thermal subsidence due to cooling of the stretched European lithosphere is recorded by the Grey Flysch Group (Ford et al., 2016; Rougier et al., 2016).

We used our β values to apply a uniform stretching model in the Aquitaine area in order to calculate postrift thermal subsidence (as implemented in Allen and Allen (2005), equations (3.16) and (3.17), p.82; McKenzie (1978). In the model, the basin deepens due to thermal cooling of the lithosphere, then is filled with sediment up to sea level, generating additional sediment load which is taken into account in the calculations. We used a standard prerift lithospheric thickness of 125 km as we assume the European lithosphere was at equilibrium. Parameters are summarized in Table 1. In this model, we assume that the postrift thermal subsidence is not affected by any changes in the thermal state of the lithosphere associated with the Pyrenean orogeny (see section 7). As the McKenzie's uniform stretching model assumed instantaneous rifting, we also do not

Table 1
Physical Parameters Used in the Calculations

Parameter	Definition	Value	Unit
α_v	Volumetric coefficient of thermal expansion	$3.28 \cdot 10^{-5}$	$^{\circ}\text{C}^{-1}$
h_{litho}	Lithospheric thickness at the onset of rifting	$125 \cdot 10^3$	m
h_{crust}	Reference crustal thickness	34	km
τ	Thermal time constant	62.8	Myr
T_m	Mantle temperature	1,333	$^{\circ}\text{C}$
ρ_d	Displaced material density	0	kg m^{-3}
ρ_l	Topographic load density	2,700	kg m^{-3}
ρ_{infill}	Basin-infill density	2,500	kg m^{-3}
ρ_{mantle}	Mantle density	3,200	kg m^{-3}
$\Delta\rho_b$	Buried load density contrast	500	kg m^{-3}
g	Gravitational acceleration	9.81	m s^{-2}
G	Gravitational constant	$6.673 \cdot 10^{-11}$	$\text{m}^3 \text{kg}^{-1} \text{s}^{-2}$
E	Young's modulus	$1 \cdot 10^{11}$	Pa
ν	Poisson's ratio	0.25	

take into account heat loss during rifting. Our calculated thermal subsidence is therefore a maximum value. Because of edge effects in the calculated β over the Grand-Rieu Ridge, the calculated thermal subsidence is overestimated south of it. Most of the thermal subsidence would have taken place during approximately 50 Myr after the initiation of rifting at 94 Ma (assuming a thermal time constant of 62.8 Myr; McKenzie, 1978). As orogenesis started at 84 Ma, thermal subsidence will therefore have continued in the foreland during convergence. We subtracted the amount of thermal subsidence from 94 to 84 Ma from total thermal subsidence (94 to present) in order to isolate the synorogenic component of the thermal subsidence (S_{to} , Figure 5d) (84 to 0 Ma). By comparing the observed thickness of synorogenic sediments (Figure 4) with these results we can make some preliminary observations that will be tested by our flexural modeling. Toward the Massif Central, recent regional uplift has impacted depth to top Paleozoic basement, and thus, the quality of β and S_{to} calculations is reduced. Results in this area must therefore be considered with caution.

In the western area, S_{to} is similar to the observed thickness of the synorogenic sediments (Figure 4), suggesting that no additional subsidence mechanism, such as orogenic loading, is required. In the central sector, S_{to} is significant in the AAC rift, reaching its maximum (3,500 m) in the Arzacq subbasin where β is highest (Figure 5c). The amount of thermal subsidence varies from 0 to 1,000 m (locally up to 1,500 m) on the northern platforms and on the Carcassonne High.

6. Flexural Modeling

We modeled the 2-D flexure of the European lithosphere as the response of a semiinfinite (i.e., broken) elastic plate to a surface topographic load. The southern edge of the European plate (the plate break, Figure 1c) was identified on two interpreted deep seismic profiles across the Pyrenees (ECORS PYRENEES: ECORS Pyrenees Team, 1988; ECORS ARZACQ: Teixell et al., 2016). By extrapolating between these control points, we defined the trace of the plate break below the AZ (Figure 1c).

We calculated the flexure along four profiles orthogonal to the Pyrenean belt (see location on Figure 1c): Profile 1 lies east of the Toulouse Fault, and Profiles 2 and 3 are located in the central sector, passing through the Saint-Gaudens and Lourdes gravity anomalies, respectively. Profile 4 lies in the western sector and passes through the Labourd gravity anomaly. These profiles provide a good representation of the key structural elements of the Aquitaine Basin.

We followed the flexure modeling method described in Contreras-Reyes and Osses (2010) (see methodology in their appendix). This calculation assumes a horizontal predeformation surface and complete sediment infill of the load-induced flexural depressions up to sea level. Physical parameters used in the calculations are listed in Table 1. Since the depth to the base of the Aquitaine foreland succession includes small-scale variations due to local thrust, fold, and salt tectonics, it was smoothed to facilitate comparison with models. We first removed the extreme effect of diapirs and then performed a local regression using weighted linear least squares and a first-degree polynomial model. We tested different values of the elastic thickness, T_e , in order to achieve the best representation of the observed flexure, keeping T_e constant or varying it along the profile. We then computed the gravity effect of the calculated flexed crust, based on the resultant anomaly of two density contrast interfaces: the calculated base of foreland basin and the flexed Moho. This technique is based on the method developed by Talwani et al. (1959) and discussed in Watts (2001). The flexed Moho, which differs from the observed Moho, is obtained by adding the thickness of the preorogenic cover and the observed crustal thickness (Figure 5b) to the calculated flexure.

6.1. Topographic Load and T_e Values

The surface topographic load that acts on the edge of the European lithosphere was defined from the topography of the Pyrenees between the plate break and the NPFT (Figure 1c). A mean density of $2,700 \text{ kg/m}^3$ was assumed for the topographic load and a mean density of $2,500 \text{ kg/m}^3$ for the sediment infill, based on well

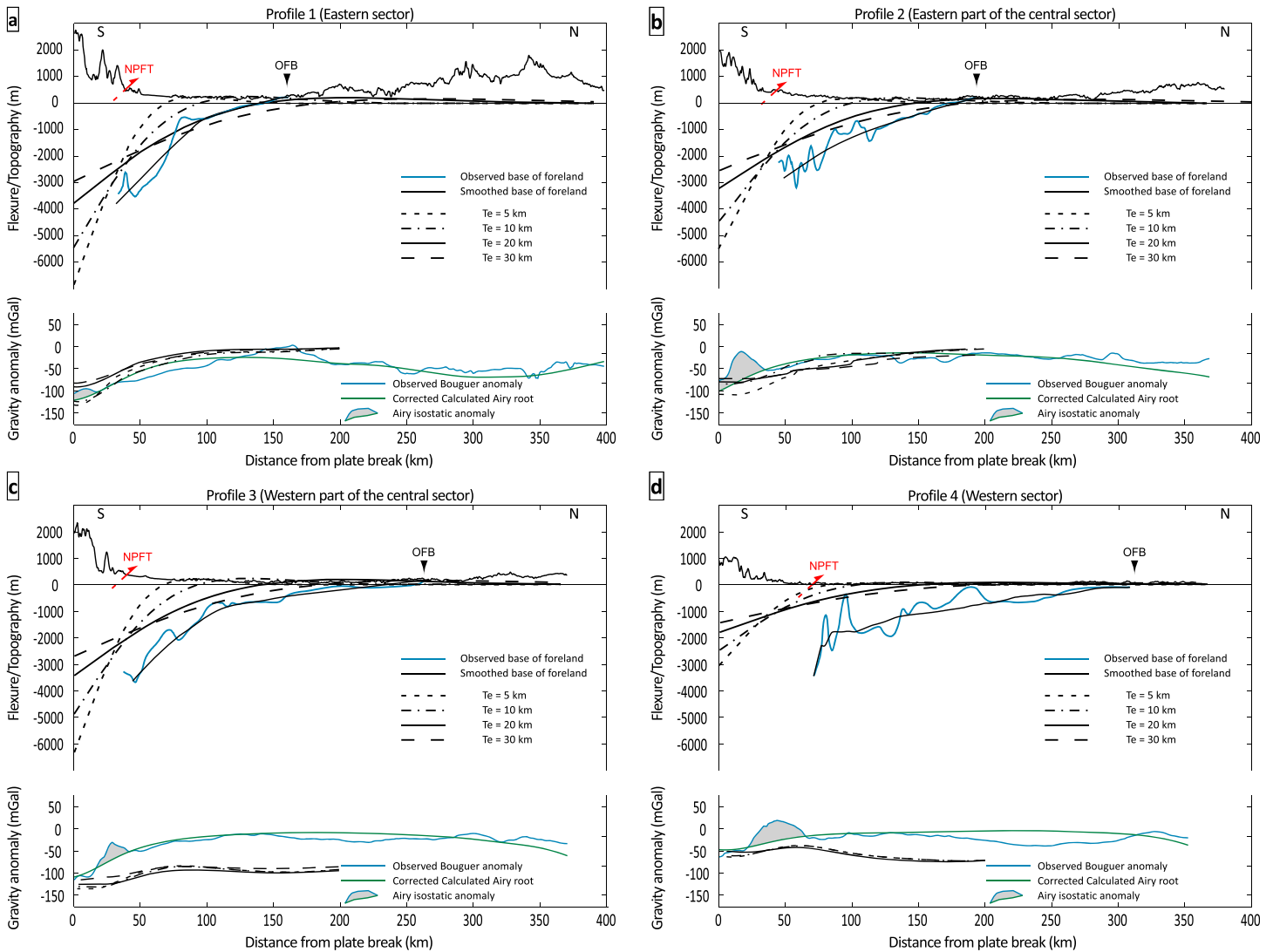


Figure 6. Observed flexure and the modeled topographic flexure for different values of T_e and the resulting Bouguer anomaly along four profiles located in Figure 1c. Results for each profile are divided into two parts. (top) Comparison of observed base of foreland (blue line) to the modeled flexure due to topographic loading only. Calculations are based on a 2-D broken plate, with the plate break located below the Axial Zone, for $T_e = 5, 10, 20,$ and 30 km. The topographic load is applied from the plate break to the NPFT. (bottom) Comparison of the predicted gravity anomalies (Airy root) based on surface loading (thick green line) to the observed Bouguer anomalies (solid blue line) and the gravity affected of the calculated flexure. Calculated gravity effects are based on calculated flexures in the upper figure. See text for details. See location of the plate break and profiles in Figure 1c. NPFT: North Pyrenean Frontal Thrust; OFB: outcropping foreland base.

log data and literature (Brunet, 1986; Ford et al., 2016). The flexure of the eastern foreland is difficult to model due to erosion of the northern basin.

Figure 6 (upper profiles) shows the topography and observed flexure (base of synorogenic succession) along the four profiles. Using a constant value of T_e along the profiles, a range of T_e values was tested (5, 10, 20, and 30 km). Irrespective of the value of T_e used, there are clearly large discrepancies between the calculated and observed flexural profiles. These discrepancies increase westward as the calculated deflection becomes significantly less than the observed flexure. A simple flexural model with constant T_e therefore cannot explain either the amplitude or the width of the synorogenic basin. A model incorporating a southward decreasing T_e , qualitatively linked to the observed variation in β (Figure 5c), with a “low” T_e for the stretched crust and a “normal” T_e in the platform was then tested (topographic load, models in Figure 7, green lines). The resulting models better approximate the shape of the observed flexure, although the magnitude of the modeled flexure is still too low.

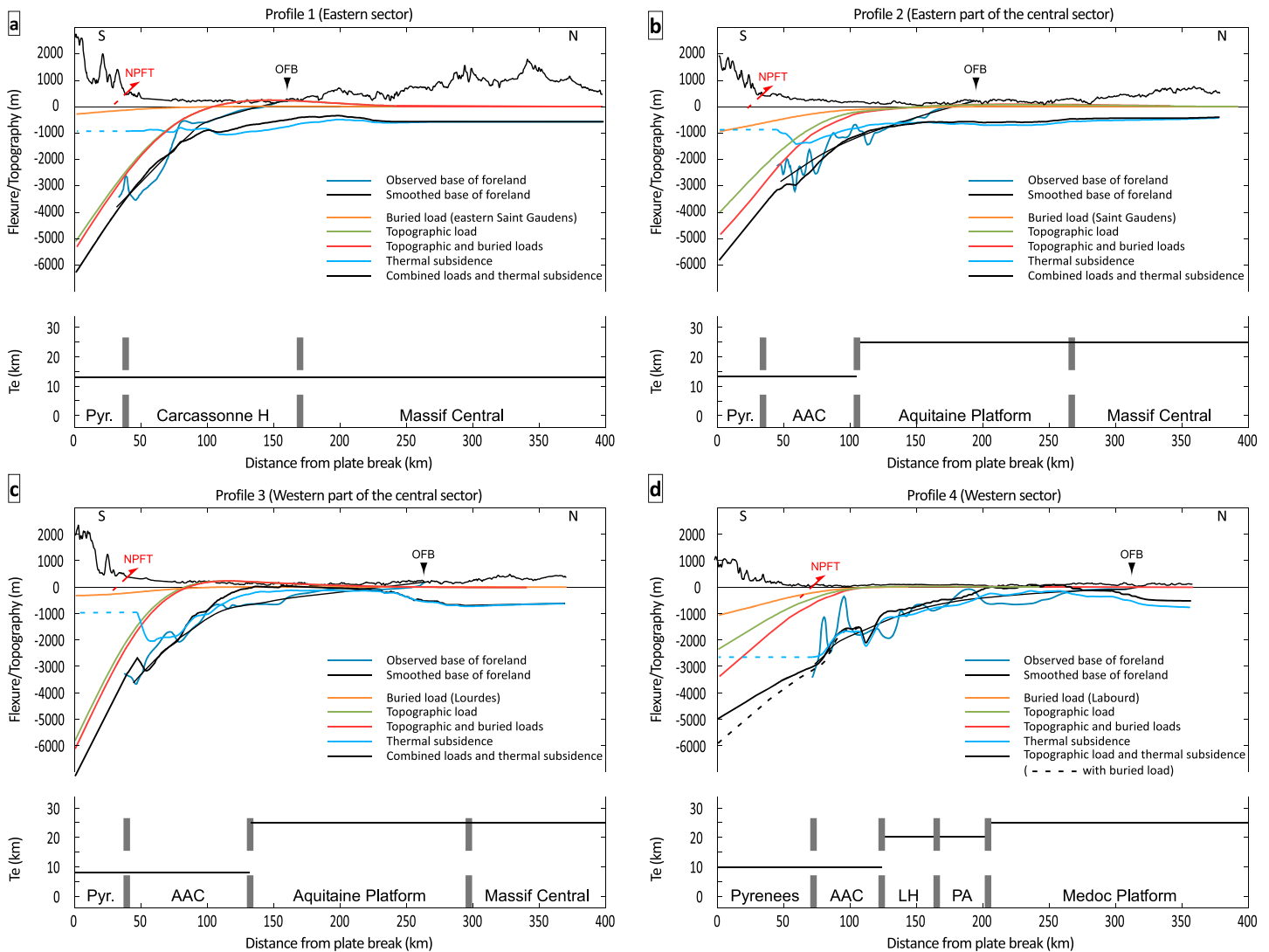


Figure 7. Observed flexure and combined modeled flexure and variations of T_e along the profiles located on Figure 1c. Results for each profile are divided into two parts. (top) Comparison of the predicted combined flexural profiles (thick black line) due to topographic (green line) and buried (orange line) loads and S_{to} (light blue line). South of the NPFT, S_{to} has been extrapolated with constant value. (bottom) T_e value used in the calculation. NPFT: North Pyrenean Frontal Thrust; OFB: outcropping foreland base; Pyr.: Pyrenees; AAC: Adour-Arzacq-Comminges; LH: Landes High; PA: Parentis. (a) Profile 1: eastern sector. (b) Profile 2: eastern part of the central sector of the Aquitaine Basin. Note that due to edge effect in the south of the S_{to} map, we remove the nonconsistent data prior to combining S_{to} with the load-induced flexural profile. (c) Profile 3: western part of the central sector of the Aquitaine Basin. (d) Profile 4: western sector. Note that the total flexure is shown with and without the effect of the Labourd buried load.

Figure 6 (bottom row) shows the observed Bouguer anomalies and the calculated Bouguer anomaly response of the previously calculated flexure. In the eastern sector and the eastern part of the central sector (Profiles 1 and 2, Figures 6a and 6b), the calculated Bouguer anomaly response of a flexure with T_e values of 10 km is in agreement with the observed anomalies. This observation is valid for the southern part only, as the northern part is disturbed by the Massif Central. To the west, the discrepancies between the observed and calculated gravity anomalies increase westward (Profiles 3 and 4, Figures 6c and 6d). This implies that the observed topography cannot replicate the observed flexure or the observed gravity highs in the NPZ.

6.2. Buried Loads

One explanation for such a discrepancy between a flexural model based on surface loading and the observed flexure in a foreland basin is the presence of buried loads (Ali & Watts, 2009; Karner & Watts, 1983; Lin & Watts,

2002; Royden & Karner, 1984). As described above, Bouguer anomaly highs along the NPZ are interpreted as due to the presence of dense bodies in the upper crust (e.g., lower crust or mantle material) in the upper crust (Casas et al., 1997; de Cabissole, 1990; Grandjean, 1994; Jammes, Lavier, et al., 2010; Pedreira et al., 2003, 2007).

We therefore evaluated the effect of buried loads associated with the Saint-Gaudens, Lourdes, and Labourd gravity anomalies on the flexure of the Aquitaine Basin (Profiles 2, 3, and 4, respectively) using the same method as in Lin and Watts (2002), among others.

We first calculated the gravity effect of the crustal root of the mountain belt assuming an Airy model with a topographic density of $2,670 \text{ kg/m}^3$ and a mantle density of $3,200 \text{ kg/m}^3$. We used a reference crustal thickness value of 34 km (see section 5.2).

We then compared the gravity effect of the calculated Airy Moho to the observed Bouguer anomaly (Figure 6, bottom). The shape of the gravity effect of the Airy Moho fits the large wavelength shape of the observed Bouguer anomaly. However, the observed gravity appears $\sim 40 \text{ mGal}$ too low compared to the calculated gravity. This is because the Bouguer anomaly includes long wavelength regional fields which have not been taken into account in the Airy isostatic calculation. An explanation is the hypothesis that the Pyrenees are overcompensated at depth (Vacher & Souriau, 2001). We therefore subtracted 40 mGal from the gravity effect of the Airy Moho prior to subtracting it from the observed Bouguer anomaly.

Finally, we used the difference between the corrected gravity effect of the Airy Moho and the observed anomaly together with the Green's equivalent layer theorem to determine the equivalent height and hence size of the buried load assuming a density contrast of 500 kg/m^3 for the material of the buried load, which corresponds to a mantle body emplaced into upper continental crust (Casas et al., 1997; de Cabissole, 1990; Grandjean, 1994; Jammes, Lavier, et al., 2010; Pedreira et al., 2003, 2007). We then calculated the additional flexure generated by these dense bodies using the calculated equivalent height as we did for the topography.

The flexure due to a buried load is represented on Figure 7 for Profiles 1 to 4 (orange lines). On Profile 1 (Figure 7a) where no Bouguer anomaly high is recognized in the NPZ, the positive part of the Airy isostatic anomaly is explained as the lateral influence of the Saint-Gaudens dense body (Figure 3), which creates a flexure of $\sim 280 \text{ m}$. On Profile 2 (Figure 7b) the buried load creates a flexure of $\sim 960 \text{ m}$. On Profile 3 (Figure 7c) the buried load creates a flexure of $\sim 340 \text{ m}$. Finally, on Profile 4 (Figure 7d), the buried load creates a flexure of $\sim 1,060 \text{ m}$. These values along are too low to account for the observed flexure.

6.3. Combining Load-Induced Subsidence With Thermal Subsidence (S_{to})

The combined effect of topographic and buried loads cannot replicate the observed base of foreland along the four profiles (Figure 7, thick black lines). Another source of subsidence is therefore required in the Aquitaine foreland basin. In this section we investigate the role S_{to} , in addition to the effect of topographic and buried loads. We assume that the synorogenic thermal subsidence S_{to} is the only additional major source of subsidence. The relatively short lag time between the end of rifting and the onset of convergence (10 Myr) would guarantee that postrift thermal subsidence continues during the early phases of orogenesis (according to parameters used in the calculations; see Table 1). As S_{to} is overestimated south of the Grand-Rieu Ridge, we discarded these data prior to integrating thermal subsidence into our calculation. We extrapolated the most southerly value of S_{to} from the southern limit of the thermal subsidence grid (Figure 5d) to the plate break to the south so that S_{to} could be added to load-generated flexural subsidence. Figure 7 shows the flexure generated by different combinations of the identified loads and S_{to} along the four sections.

In the eastern sector, (Profile 1, Figure 7a), the lateral influence of the Saint-Gaudens dense body is rather small and contributes little to the load. S_{to} is also minor in this area. The combined effect of topographic and buried loads and S_{to} reproduces the amplitude of the southern part of the observed foreland flexure with a T_e of 13 km. As explained above, this profile is incomplete because the northern foreland was eroded during late uplift of the Massif Central. An uncertainty must therefore be assigned to this model, in particular, to the very low value of T_e , which is clearly inconsistent with a nonrifted crust.

In the eastern part of the central sector (Profile 2, Figure 7b), the Saint-Gaudens buried load is an important component (about a third) of the combined load, which is nevertheless too small to replicate the

observed flexure. By adding the S_{to} we can reproduce the amplitude of the observed flexure. The best fit uses a T_e of 14 km in the AAC rift and 25 km in the Aquitaine Platform. Because of postorogenic uplift, the basal foreland units crop out ~145 km north of the NPFT. We therefore cannot directly compare the location of the forebulge. Nevertheless, it appears to fit with the forebulge location projected in from the west (Figure 4).

In the western part of the central sector, directly north of the Lourdes anomaly (Profile 3, Figure 7c), the combined effect of topographic and buried loads is again too small to replicate the base of the foreland succession. The effect of the Lourdes dense body load is small compared to the topographic load. The combined load and S_{to} , however, reproduces the observed flexure. The best fit uses a T_e of 7 km in the AAC rift and 25 km in the Aquitaine Platform. From ~80 to 145 km north of the NPFT, the modeled flexure is not deep enough compared to the observed base of the foreland basin (discrepancy of ~800 m).

Finally, in the western sector (Profile 4, Figure 7d), S_{to} alone is in the range of the base of the foreland succession. North of the NPFT, the topographic flexure can be added to the S_{to} and the combined curve is still consistent with the observed base of foreland basin. Although the nature of the Labourd dense body is matter of debate (see section 3), we tested the influence of this dense body. We cannot, however, derive a clear conclusion, as it is not required to explain observed subsidence in the foreland basin. The best fit uses a $T_e = 10$ km in the AAC, 15 km in the Landes High, and 20 km in the Medoc Platform. The profile passes through the eastern margin of the Parentis rift. T_e variations in this area do not produce significant changes; we therefore used the same values as for the Landes High. However, derived T_e values in this sector have little significance as subsidence is mainly due to S_{to} .

7. Discussion

7.1. Crustal Inheritance

The Aquitaine Basin is an excellent example of a retro-foreland basin that was superimposed on a young, highly segmented rift system, which controlled foreland behavior. We have shown that the flexure of the Aquitaine Basin can be accounted for by a model combining surface and subsurface loads with tectonic thermal subsidence linked to preorogenic rifting. There are, however, strong lateral variations. The preserved eastern foreland basin is superimposed on unstretched crust, while in the central and western sectors, the basin is superimposed on stretched crust.

The geometry of the Early Cretaceous rift system is still debated (e.g., Clerc & Lagabrielle, 2014; DebRoas, 1987, 1990; Masini et al., 2014; Teixell et al., 2016; Tugend et al., 2014). Rifting created a complex distribution of depocenters now preserved both in the foreland and in the NPZ where they are strongly inverted (e.g., DebRoas, 1987, 1990; Masini et al., 2014). Subcontinental mantle was exhumed below some rift-basins now preserved in the NPZ, recording an overall southward increase in crustal thinning of the European margin (e.g., Lagabrielle & Bodinier, 2008; Lherz rift-basin, Clerc et al., 2012; Mauléon rift-basin, Masini et al., 2014; Tugend et al., 2014). Major transverse crustal structures, probably Variscan in origin, partitioned the Aptian-Cenomanian rifting (e.g., Boillot, 1986; DebRoas, 1990; Larrasoana et al., 2003; Tugend et al., 2014), notably the Pamplona Fault in the western Pyrenees and the Toulouse Fault and the newly defined ECL in the eastern retro-foreland (Figure 5). This segmentation continues offshore (Carola et al., 2013; Ferrer et al., 2008; Roca et al., 2011; Tugend et al., 2014).

While coherent with the work of Tugend et al. (2014), we provide a more detailed insight into the southwest European crustal geometry and stretching in the Pyrenean retro-foreland (Figure 5). New mapping of foreland crustal thickness shows that Aptian-Cenomanian stretching increased westward and southward across a segmented crust. Our derived stretching values are in the range of those of Tugend et al. (2014) for the southwest Aquitaine Basin. Figure 5c shows that within the AAC rift stretching and basin geometry are highly heterogeneous. Our data clearly define the northern limit of rifting in the west and central foreland and show that it stepped south to the east of the Toulouse Fault where it is integrated into the orogen. Paleozoic blocks (e.g., the Landes High and the Grand-Rieu Ridge) and transverse faults (i.e., Toulouse Fault and ECL) separate rift depocenters. This broad NE-SW segmentation pattern associated with a regional eastward southstepping of depocenters is consistent with the more local “en-échelon” geometry proposed by DebRoas (1987, 1990) in the NPZ.

The ECL clearly controlled the geometry of the foreland. In contrast, the Toulouse Fault was inactive during convergence as it cannot be identified on the foreland basin isopach map (Figure 4). Farther west, the very heterogeneous geometry of the foreland basin, probably due to salt tectonics, obscures any smaller scale segmentation of the foreland. The Pamplona Fault does not appear to cut the Aquitaine Basin. It affected only the southern Pyrenees and the NPZ during both rifting and convergence, when it transferred shortening farther south in the Iberian plate (Larrasoana et al., 2003).

T_e can be considered as a proxy for the long-term strength of the lithosphere and may therefore be indirectly correlated to the amount of stretching experienced by the plate, if thermal reequilibration has not been achieved at the time of loading (Iberian plate, southern Pyrenees, Gaspar-Escribano et al., 2001; Zoetemeijer et al., 1990; European plate, western Alps, Stewart & Watts, 1997). This relationship is supported by our analysis of the Aquitaine Basin where low T_e values are valid for areas affected by lithospheric thinning. In the Aquitaine Basin, the decrease in T_e toward the west and toward the south (7–25 km, Figure 7) is correlated to an increase in β (Figure 5c). However, as flexural loading in this basin is not solely responsible for driving subsidence, it becomes difficult to constrain values of T_e with more certainty. Our values, however, are in the same range as those proposed for the western European plate by Desegaulx et al. (1990) and Karner and Watts (1983) (15 to 20 km and 25 km, respectively), and for other foreland basins that are superimposed on relatively young passive margins, such as Taiwan (13 km) (Lin & Watts, 2002).

Fosdick et al. (2014) propose that an inherited passive margin geometry may localize or “trap” the main depocenter of a foreland basin at its initiation, using the Magallanes retro-arc foreland basin as a case study. The position of the central Aquitaine Basin above the AAC rift basin may suggest a similar localization role for the inherited rift. However, foreland basins that develop on the retro side of the orogen are characterized by relative immobility; that is, they do not migrate significantly outward (Naylor & Sinclair, 2008). As the Aquitaine Basin is a retro-foreland basin (as is the Magallanes Basin), it is therefore difficult to evaluate the true role of the inherited rift in localizing the main depocenter. However, we show that the postrift thermal subsidence is another mechanism that must be considered: the Aquitaine foreland basin is a particular case where its position in the western sector is dictated by thermal cooling above the rift.

Along strike variations in deformation style in the Aquitaine foreland can also be linked to inherited mechanical and structural properties of the crust as observed in other orogens (e.g., Kley et al., 1999). In the eastern foreland minor Eocene shortening gently reactivates the Variscan nappe stack to form basement-cored anticlines (Ford et al., 2016). West of the ECL/Toulouse Fault system inherited extensional structures are inverted below an efficient decoupling horizon along Keuper evaporites with deforming sedimentary cover above (Rougier et al., 2016; Teixell et al., 2016).

7.2. Subsidence Mechanisms

The nonuniqueness of flexural modeling and subsidence analysis may represent a challenge when attempting to discriminate modes of subsidence. We have identified three main contributors to foreland basin subsidence, topography load, buried loads, and postrift thermal subsidence. However, other phenomena may have also contributed to subsidence including inherited bathymetry, slab pull, and dynamic subsidence. The potential role of each of these is considered below.

Although the three established subsidence mechanisms for the Aquitaine Basin operate over similar wavelengths and time scales, their respective peak of activity differs in time. Postrift thermal subsidence was mainly active during the early phase of convergence (Campanian to Eocene) while the main topographic loading occurred during Eocene collision. We suggest that loading by the buried dense bodies occurred contemporaneously with topographic loading as they were emplaced into the upper crust during main collision. As we have analyzed only the present-day configuration of the Aquitaine Basin, we cannot perform a more detailed analysis of the evolution of these mechanisms through time.

Our model for the Aquitaine Basin also assumes that the load acts on a horizontal predeformation surface at 0 altitude and therefore ignores preexisting bathymetry at the onset of orogeny, which is a simplification. In Campanian times, sedimentation was deep marine in the southern part of the studied area. It would be an interesting improvement to test the effect of inherited bathymetry on the calculated flexure. Stockmal and Beaumont (1987) propose that preexisting bathymetry at the onset of orogenesis reduces the topography needed above sea level. Taking this into consideration, our model overestimates the required load.

On the southern side of the orogen, the eastern Ebro pro-foreland basin is explained by Gaspar-Escribano et al. (2001) by a combination of topographic loading and pull exerted by the downgoing Iberian plate. While slab-pull mainly affects the pro-foreland basin, the retro-foreland basin would be subjected to dynamic subsidence resulting from slab pull (DeCelles & Giles, 1996). If dynamic subsidence affected the retro-foreland, we would expect the discrepancy between the observed and calculated flexure to be greater to the east, where estimates of Pyrenean shortening and topography are higher than the western Pyrenees (see section 2.1). In the upper plate we show that topography seems to be the main controlling factor of the flexure of the eastern Aquitaine foreland basin, despite uncertainties in the T_e value (see section 6.3). We have also shown that the topographic flexure decreases westward (Figures 6 and 7), thus supporting a westward decrease in Pyrenean shortening. A significant additional source of subsidence is required in the central and western Aquitaine Basin, which we identify as due to postrift cooling.

While it is not possible to completely rule out the role of dynamic subsidence during the evolution of the Aquitaine Basin, we believe it played only a minor role. An explanation could be that the very heterogeneous geometry of the European Moho along the orogen (e.g., Chevrot et al., 2015; Wang et al., 2016) may have disturbed or inhibited convection in the mantle wedge.

We have established that postrift thermal subsidence was a major component of synorogenic subsidence in the central Aquitaine Basin and probably the principal component in the western basin. This model assumes that the foreland lithosphere was not thermally affected by crustal thickening during early convergence. Current reconstructions indicate that crustal thickening occurred during the main Eocene continental collision with little thickening during the early convergence phase (Late Cretaceous; Ford et al., 2016; Mouthereau et al., 2014). In addition, as discussed above, total shortening in the retrowedge is very small, especially in the retro-foreland (5 km, Ford et al., 2016; 6.7 km, Rougier et al., 2016). We therefore argue that, as postrift thermal subsidence was active (and decreasing) from Campanian to Eocene, any orogenic changes in the thermal state of the foreland lithosphere were minor and initiated toward the end of active thermal subsidence.

As shown by our case study, postrift thermal subsidence can play an important role in foreland basin behavior. Most studies of foreland basins developed on rifted lithosphere do not consider postrift thermal subsidence as an additional driving force of foreland subsidence. When both pro and retro-foreland basins initiate long after the end of rifting (e.g., Alps, 130 Myr, Stewart & Watts, 1997; Papua New-Guinea, 120 Myr, Haddad & Watts, 1999; Southern Andes, 80 Myr, Fosdick et al., 2014), the lithosphere has time to thermally reequilibrate and no effect of postrift thermal subsidence needs to be added to the flexural subsidence. In the Taiwan orogenic system, the end of rifting and initiation of the pro-foreland basin are separated by only 24 Myr. We would therefore expect postrift thermal cooling to contribute to foreland subsidence. Lin and Watts (2002), however, explain the observed foreland subsidence as a combination of topographic and buried loads using relatively low T_e values. One possibility would be that the authors have overlooked the effect of postrift thermal subsidence, by underestimating T_e and hence reducing the load required to flex the plate. As their estimates of T_e are robust and Taiwan is associated with active subduction, another possibility is that the thermal regime of the lithosphere is disturbed by the cold downgoing slab.

8. Conclusions

The geometry and evolution of foreland basins provide some of the best evidence on the thermal and mechanical properties and behavior of the continental lithosphere. A new analysis of the crustal geometry, foreland succession, Bouguer anomalies, and flexural behavior of the Aquitaine retro-foreland basin reveals the following characteristics.

Early Cretaceous rifting strongly influenced the evolution of the Aquitaine Basin. The rifting ended only 10 Myr before the onset of orogenesis, and created a highly segmented rift system. Major oblique faults segment the European crust and contribute to along- and across-strike variations in crustal stretching. Overall β increases westward. This inheritance influenced the foreland basin behavior in two ways: (1) by generating postrift thermal subsidence that was partially synchronous with Pyrenean convergence and (2) by creating lateral variations in T_e values in the variably thinned European plate. T_e seems linked with the stretching of the crust: the lower the T_e , the higher the β .

Numerical modeling of the flexure of the European plate shows that (1) in the east, the topographic load of the Pyrenean orogen may be the main source of subsidence; (2) in the center, the combined effect of topographic load, buried load, and postrift thermal subsidence can satisfactorily explain the geometry of the foreland basin; and (3) in the west, the foreland basin geometry is mainly controlled by thermal subsidence.

In conclusion, this case study in the Pyrenees demonstrates that postrift thermal subsidence can play an important role in foreland basin behavior. The possibility of active thermal subsidence during convergence should be considered in all foreland case studies.

Acknowledgments

This work was funded by PhD grant of Paul Angrand as a part of the BRGM (Bureau des Ressources Géologiques et Minières) RGF (Référentiel Géologique de la France) Pyrénées Program and a grant from the Région Lorraine. The data used are listed in the references, tables, and shown in the figures. The authors thank B. Horton and an anonymous reviewer for constructive comments that helped us improve the original manuscript. The BGI and BRGM are acknowledged for providing gravity data and depth to Moho data, respectively. We thank Anne-Gaëlle Bader, Cédric Carpentier, Frédéric Christophoul, Dominique Frizon de Lamotte, Jérôme Sophie Leleu, Laurent Jolivet, Guillaume Martelet, Mark Naylor, and Hugh Sinclair, and colleagues at the CRPG and in the RGF Pyrénées Program for their help and fruitful discussions. The map figures were constructed using GMT (Wessel & Smith, 1991). CRPG publication number 2533.

References

- Albarède, F., & Michard-Vitrac, A. (1978). Age and significance of the North Pyrenean metamorphism. *Earth and Planetary Science Letters*, 40(3), 327–332. [https://doi.org/10.1016/0012-821X\(78\)90157-7](https://doi.org/10.1016/0012-821X(78)90157-7)
- Ali, M. Y., & Watts, A. B. (2009). Subsidence history, gravity anomalies and flexure of the United Arab Emirates (UAE) foreland basin. *GeoArabia*, 14(2), 17–44.
- Ali, M. Y., Watts, A. B., & Farid, A. (2014). Gravity anomalies of the United Arab Emirates: Implications for basement structures and infra-Cambrian salt distribution. *GeoArabia*, 19(1), 85–112.
- Allen, P. A., & Allen, J. R. (2005). *Basin analysis: Principles and applications* (2nd ed.). Oxford, UK: Blackwell Publishing Ltd.
- Beaumont, C. (1981). Foreland basins. *Geophysical Journal of the Royal Astronomical Society*, 65, 291–329. <https://doi.org/10.1002/9781444303810>
- Beaumont, C., Muñoz, J. A., Hamilton, J., & Fullsack, P. (2000). Factors controlling the Alpine evolution of the central Pyrenees inferred from a comparison of observations and geodynamical models. *Journal of Geophysical Research*, 105(B4), 8121–8145. <https://doi.org/10.1029/1999JB900390>
- Biteau, J.-J., Le Marrec, A., Le Vot, M., & Masset, J.-M. (2006). The Aquitaine Basin. *Petroleum Geoscience*, 12(3), 247–273. <https://doi.org/10.1144/1354-079305-674>
- Boillot, G. (1986). Comparison between the Galicia and Aquitaine margins. *Tectonophysics*, 129(1-4), 243–255. [https://doi.org/10.1016/0040-1951\(86\)90254-4](https://doi.org/10.1016/0040-1951(86)90254-4)
- Bois, C., & ECORS Scientific Party (1990). Major geodynamic processes studied from the ECORS deep seismic profiles in France and adjacent areas. *Tectonophysics*, 173, 397–410. [http://doi.org/10.1016/0040-1951\(90\)90233-X](http://doi.org/10.1016/0040-1951(90)90233-X)
- Bourrouilh, R., Richert, J.-P., & Zolnai, G. (1995). The north Pyrenean Aquitaine Basin, France: Evolution and hydrocarbons. *AAPG Bulletin*, 79(6), 831–853.
- BRGM, Elf, Esso, & SNPA (1974). *Géologie du Bassin d'aquitaine* (BRGM Ed). Paris: BRGM Editions.
- Brunet, M.-F. (1986). The influence of the evolution of the Pyrenees on adjacent basins. *Tectonophysics*, 129(1-4), 343–354. [https://doi.org/10.1016/0040-1951\(86\)90260-X](https://doi.org/10.1016/0040-1951(86)90260-X)
- Brunet, M.-F. (1994). Subsidence in the Parentis basin (Aquitaine, France): Implication of the thermal evolution. In *Hydrocarbon and petroleum geology of France* (pp. 187–198). Berlin, Heidelberg: Springer.
- Burov, E. B., & Diament, M. (1995). The effective elastic thickness (Te) of continental lithosphere: What does it really mean? *Journal of Geophysical Research*, 100(B3), 3905–3927. <https://doi.org/10.1029/94JB02770>, Retrieved from <http://www.gfd.geophys.ethz.ch/~kausb/Teaching/DynLithMantle/papers/94JB02770.pdf>
- Canérot, J., Hudec, M. R., & Rockenbauch, K. (2005). Mesozoic diapirism in the Pyrenean orogen: Salt tectonics on a transform plate boundary. *AAPG Bulletin*, 89(2), 211–229. <https://doi.org/10.1306/09170404007>
- Carola, E., Tavani, S., Ferrer, O., Granado, P., Quintà, A., Butillé, M., & Muñoz, J. A. (2013). Along-strike extrusion at the transition between thin- and thick-skinned domains in the Pyrenean Orogen (northern Spain). *Geological Society, London, Special Publications*, 377(1), 119–140. <https://doi.org/10.1144/SP377.3>
- Casas, A., Kearey, P., River, L., & Adam, C. R. (1997). Gravity anomaly map of the Pyrenean region and a comparison of the deep geological structure of the western and eastern Pyrenees. *Earth and Planetary Science Letters*, 150(1-2), 65–78. [https://doi.org/10.1016/S0012-821X\(97\)00087-3](https://doi.org/10.1016/S0012-821X(97)00087-3)
- Chevrot, S., Sylvander, M., Diaz, J., Ruiz, M., & Paul, A. (2015). The Pyrenean architecture as revealed by teleseismic P-to-S converted waves recorded along two dense transects. *Geophysical Journal International*, 200(2), 1094–1105. <http://doi.org/10.1093/gji/ggu400>
- Chevrot, S., Villaseñor, A., Sylvander, M., Benahmed, S., Beucler, E., Cougoulat, G., ... Wolyniec, D. (2014). High-resolution imaging of the Pyrenees and massif central from the data of the PYROPE and IBERARRAY portable array deployments. *Journal of Geophysical Research: Solid Earth*, 119, 6399–6420. <https://doi.org/10.1002/2014JB010953>
- Choukroune, P., & Mattauer, M. (1978). Tectonique des plaques et Pyrénées: sur le fonctionnement de la faille transformante nord-pyrénéenne; comparaisons avec des modèles actuels. *Bulletin de la Société Géologique de France*, 7(5), 689–700. <https://doi.org/10.2113/gssgfbull.57-XX.5.689>
- Choukroune, P., & ECORS Pyrenees Team (1989). The ECORS Pyrenean deep seismic profile reflection data and the overall structure of an orogenic belt. *Tectonics*, 8(1), 23–39. <https://doi.org/10.1029/TC008i001p00023>
- Choukroune, P., Roure, F., & Pinet, B. (1990). Main results of the ECORS Pyrenees profile. *Tectonophysics*, 173(1-4), 411–423. [https://doi.org/10.1016/0040-1951\(90\)90234-Y](https://doi.org/10.1016/0040-1951(90)90234-Y)
- Christophoul, F., Soula, J. C., Brusset, S., Elibana, B., Roddaz, M., Bessiere, G., & Déramond, J. (2003). Time, place and mode of propagation of foreland basin systems as recorded by the sedimentary fill: Examples of the Late Cretaceous and Eocene retro-foreland basins of the north-eastern Pyrenees. *Geological Society, London, Special Publications*, 208(1), 229–252. <https://doi.org/10.1144/GSL.SP.2003.208.01.11>
- Clerc, C., & Lagabrielle, Y. (2014). Thermal control on the modes of crustal thinning leading to mantle exhumation: Insights from the Cretaceous Pyrenean hot paleomargins. *Tectonics*, 33(7), 1340–1359. <https://doi.org/10.1002/2013TC003471>
- Clerc, C., Lagabrielle, Y., Neumaier, M., Reynaud, J. Y., & De Saint Blanquat, M. (2012). Exhumation of subcontinental mantle rocks: Evidence from ultramafic-bearing clastic deposits nearby the Lherz peridotite body, French Pyrenees. *Bulletin de la Société Géologique de France*, 183(5), 443–459. <https://doi.org/10.2113/gssgfbull.183.5.443>
- Contreras-Reyes, E., & Osses, A. (2010). Lithospheric flexure modelling seaward of the Chile trench: Implications for oceanic plate weakening in the trench outer rise region. *Geophysical Journal International*, 182(1), 97–112. <https://doi.org/10.1111/j.1365-246X.2010.04629.x>
- Curnelle, R. (1983). Evolution structuro-sédimentaire du Trias et de l'Infra-Lias d'Aquitaine. *Bulletin des Centres de Recherches Exploration-Production Elf-Aquitaine*, 7(1), 69–99.

- Daignières, M., De Cabissole, B., Gallart, J., Hirn, A., Surinach, E., & Torné, M. (1989). Geophysical constraints on the deep structure along the ECORS PYRENEES line. *Tectonics*, 8(5), 1051–1058. <https://doi.org/10.1029/TC008i005p01051>
- Daignières, M., Gallart, J., Banda, E., & Hirn, A. (1982). Implications of the seismic structure for the orogenic evolution of the Pyrenean range. *Earth and Planetary Science Letters*, 57(1), 88–100. [https://doi.org/10.1016/0012-821X\(82\)90175-3](https://doi.org/10.1016/0012-821X(82)90175-3)
- Daignières, M., Gallart, J., & Hirn, A. (1981). Etude sismique des Pyrénées. Apport à la géodynamique. *Bulletin Du BRGM*, 2, 83–92.
- Daignières, M., Séguret, M., Specht, M., & ECORS Team (1994). The Arzacq-western Pyrenees ECORS deep seismic profile. In *Hydrocarbon and petroleum geology of France* (pp. 199–208). Berlin, Heidelberg: Springer. https://doi.org/10.1007/978-3-642-78849-9_15
- de Cabissole, B. (1990). *Apport des données gravimétriques à la connaissance de a chaîne des Pyrénées le long du profil ECORS*. Université de Montpellier.
- Debroas, E.-J. (1987). Modèle de bassin triangulaire à l'intersection de décrochements divergents pour le fossé albo-cénomaniens de la Ballongue. *Bulletin de la Société Géologique de France*, 8(5), 887–898.
- Debroas, E.-J. (1990). Le Flysch noir albo-cénomaniens témoin de la structuration albienne à sénonienne de la Zone nord-pyrénéenne en Bigorre (Hautes-Pyrénées, France). *Bulletin de La Société Géologique de France*, 8(2), 273–285.
- DeCelles, P. G. (2012). Foreland basin systems revisited: Variations in response to tectonic settings. In C. Busby & A. Azor (Eds.), *Tectonics of Sedimentary Basins: Recent Advances* (pp. 405–426). Oxford, UK: Blackwell Publishing Ltd. <https://doi.org/10.1002/9781444347166.ch20>
- DeCelles, P. G., Carrapa, B., Horton, B. K., & Gehrels, G. E. (2011). Cenozoic foreland basin system in the central Andes of northwestern Argentina: Implications for Andean geodynamics and modes of deformation. *Tectonics*, 30, TC6013. <https://doi.org/10.1029/2011TC002948>
- DeCelles, P. G., & Giles, K. a. (1996). Foreland basin systems. *Basin Research*, 8(2), 105–123. <https://doi.org/10.1046/j.1365-2117.1996.01491.x>
- DeCelles, P. G., & Horton, B. K. (2003). Early to middle Tertiary foreland basin development and the history of Andean crustal shortening in Bolivia. *Geological Society of America Bulletin*, 115(1), 58–77. [https://doi.org/10.1130/0016-7606\(2003\)115%3C0058:ETMTFB%3E2.0.CO;2](https://doi.org/10.1130/0016-7606(2003)115%3C0058:ETMTFB%3E2.0.CO;2)
- Demange, M., & Jamet, P. (1986). L'accident majeur Mazamet-Tantajo (Montagne noire): décrochement tardi-hercynien et faille inverse pyrénéenne. *Géologie de la France*, 3, 273–280.
- Desegaulx, P., & Brunet, M.-F. (1990). Tectonic subsidence of the Aquitaine Basin since Cretaceous times. *Bulletin de La Société Géologique de France*, 8(2), 295–306.
- Desegaulx, P., Kooi, H., & Cloetingh, S. (1991). Consequences of foreland basin development on thinned continental lithosphere: Application to the Aquitaine Basin (SW France). *Earth and Planetary Science Letters*, 106(1–4), 116–132. [https://doi.org/10.1016/0012-821X\(91\)90067-R](https://doi.org/10.1016/0012-821X(91)90067-R)
- Desegaulx, P., Roure, F., & Villein, A. (1990). Structural evolution of the Pyrenees: Tectonic inheritance and flexural behaviour in the continental crust. *Tectonophysics*, 182(3–4), 211–225. [https://doi.org/10.1016/0040-1951\(90\)90164-4](https://doi.org/10.1016/0040-1951(90)90164-4)
- Dickinson, W. R. (1974). Plate tectonics and sedimentation. In *Special Publication - Society of Economic Paleontologists and Mineralogists* (Vol. 22, pp. 1–27). Retrieved from <http://search.ebscohost.com/login.aspx?direct=true&AuthType=ip,url,uid&db=geh&AN=1975-007806&lang=fr&site=eds-live>
- ECORS Pyrenees Team (1988). The ECORS deep reflection seismic survey across the Pyrenees. *Nature*, 331(6156), 508–511. <https://doi.org/10.1038/331508a0>
- Fabriès, J., Lorand, J.-P., & Bodinier, J.-L. (1998). Petrogenetic evolution of orogenic Iherzolite massifs in the central and western Pyrenees. *Tectonophysics*, 292(1–2), 145–167. [https://doi.org/10.1016/S0040-1951\(98\)00055-9](https://doi.org/10.1016/S0040-1951(98)00055-9)
- Ferrer, O., Jackson, M. P. A., Roca, E., & Rubinat, M. (2012). Evolution of salt tectonics during extension and inversion of the offshore Parentis Basin (Eastern Bay of Biscay). *Geological Society, London, Special Publications*, 363(1), 361–380. <https://doi.org/10.1144/SP363.16>
- Ferrer, O., Roca, E., Benjumea, B., Muñoz, J. A., Ellouz, N., & MARCONI Team (2008). The deep seismic reflection MARCONI-3 profile: Role of extensional Mesozoic structure during the Pyrenean contractional deformation at the eastern part of the Bay of Biscay. *Marine and Petroleum Geology*, 25(8), 714–730. <https://doi.org/10.1016/j.marpetgeo.2008.06.002>
- Fitzgerald, P. G., Muñoz, J. A., Coney, P. J., & Baldwin, S. L. (1999). Asymmetric exhumation across the Pyrenean orogen: Implications for the tectonic evolution of a collisional orogen. *Earth and Planetary Science Letters*, 173(3), 157–170. [https://doi.org/10.1016/S0012-821X\(99\)00225-3](https://doi.org/10.1016/S0012-821X(99)00225-3)
- Ford, M., Duchene, S., Gasquet, D., & Vanderhaeghe, O. (2006). Two-phase orogenic convergence in the external and internal SW Alps. *Journal of the Geological Society*, 163(5), 815–826. <https://doi.org/10.1144/0016-76492005-034>
- Ford, M., Hemmer, L., Vacherat, A., Gallagher, K., & Christophoul, F. (2016). Retro-wedge foreland basin evolution along the ECORS line, eastern Pyrenees, France. *Journal of the Geological Society*, 173(3), 419–437. <https://doi.org/10.1144/jgs2015-129>
- Fosdick, J. C., Graham, S. A., & Hilley, G. E. (2014). Influence of attenuated lithosphere and sediment loading on flexure of the deep-water Magallanes retroarc foreland basin, southern Andes. *Tectonics*, 33, 2505–2525. <https://doi.org/10.1002/2014TC003684>
- Gallart, J., Diaz, J., Nercessian, A., Mauffret, A., & Dos Reis, T. (2001). The eastern end of the Pyrenees: Seismic features at the transition to the NW Mediterranean. *Geophysical Research Letters*, 28(11), 2277–2280. <https://doi.org/10.1029/2000GL012581>
- García-Castellanos, D., Fernández, M., & Torné, M. (2002). Modeling the evolution of the Guadalquivir foreland basin (southern Spain). *Tectonics*, 21(3), 1018. <https://doi.org/10.1029/2001TC001339>
- Gaspar-Escribano, J. M., van Wees, J. D., ter Voorde, M., Cloetingh, S., Roca, E., Cabrera, L., ... García-Castellanos, D. (2001). Three-dimensional flexural modelling of the Ebro Basin (NE Iberia). *Geophysical Journal International*, 145(2), 349–367. <https://doi.org/10.1046/j.1365-246x.2001.01379.x>
- Golberg, J. M., & Leyreloup, A. F. (1990). High temperature-low pressure Cretaceous metamorphism related to crustal thinning (Eastern North Pyrenean Zone, France). *Contributions to Mineralogy and Petrology*, 104(2), 194–207. <https://doi.org/10.1007/BF00306443>
- Grandjean, G. (1994). Etude des structures crustales dans une portion de chaîne et leur application aux Pyrénées occidentales. *Bulletin Des Centres de Recherche Exploration-Production Elf-Aquitaine*, 18(2), 2–30.
- Gunnell, Y., Zeyen, H., & Calvet, M. (2008). Geophysical evidence of a missing lithospheric root beneath the eastern Pyrenees: Consequences for postorogenic uplift and associated geomorphic signatures. *Earth and Planetary Science Letters*, 276(3–4), 302–313. <https://doi.org/10.1016/j.epsl.2008.09.031>
- Haddad, D., & Watts, A. B. (1999). Subsidence history, gravity anomalies, and flexure of the northeast Australian margin in Papua New Guinea. *Tectonics*, 18(5), 827–842. <https://doi.org/10.1029/1999TC900009>
- Henry, P., Azambre, B., Montigny, R., Rossy, M., & Stevenson, R. K. (1998). Late mantle evolution of the Pyrenean sub-continental lithospheric mantle in the light of new ⁴⁰Ar-³⁹Ar and Sm-Nd ages on pyroxenites and peridotites (Pyrenees, France). *Tectonophysics*, 296(1–2), 103–123. [https://doi.org/10.1016/S0040-1951\(98\)00139-5](https://doi.org/10.1016/S0040-1951(98)00139-5)
- Horton, B. K., & DeCelles, P. G. (1997). The modern foreland basin system adjacent to the Central Andes. *Geology*, 25(10), 895–898. [https://doi.org/10.1130/0091-7613\(1997\)025%3C0895:TMFBSA%3E2.3.CO;2](https://doi.org/10.1130/0091-7613(1997)025%3C0895:TMFBSA%3E2.3.CO;2)

- Horton, B. K., Fuentes, F., Boll, A., Starck, D., Ramirez, S. G., & Stockli, D. F. (2016). Andean stratigraphic record of the transition from backarc extension to orogenic shortening: A case study from the northern Neuquén Basin, Argentina. *Journal of South American Earth Sciences*, *71*, 17–40. <https://doi.org/10.1016/j.jsames.2016.06.003>
- Ingersoll, R. V. (1988). Tectonics of sedimentary basins. *Geological Society of America Bulletin*, *100*(11), 1704–1719. [https://doi.org/10.1130/0016-7606\(1988\)100%3C1704:TOSB%3E2.3.CO;2](https://doi.org/10.1130/0016-7606(1988)100%3C1704:TOSB%3E2.3.CO;2)
- James, V., & Canérot, J. (1999). Diapirisme et structuration post-triasique des Pyrénées occidentales et de l'Aquitaine méridionale (France). *Ecolae Geologicae Helvetiae*, *92*, 63–72.
- Jammes, S., Lavier, L., & Manatschal, G. (2010). Extreme crustal thinning in the Bay of Biscay and the western Pyrenees: From observations to modeling. *Geochemistry, Geophysics, Geosystems*, *11*, Q10016. <https://doi.org/10.1029/2010GC003218>
- Jammes, S., Manatschal, G., & Lavier, L. (2010). Interaction between prerift salt and detachment faulting in hyperextended rift systems: The example of the Parentis and Mauléon basins (Bay of Biscay and western Pyrenees). *AAPG Bulletin*, *94*(7), 957–975. <https://doi.org/10.1306/12090909116>
- Jammes, S., Manatschal, G., Lavier, L., & Masini, E. (2009). Tectosedimentary evolution related to extreme crustal thinning ahead of a propagating ocean: Example of the western Pyrenees. *Tectonics*, *28*, TC4012. <https://doi.org/10.1029/2008TC002406>
- Jammes, S., Tiberi, C., & Manatschal, G. (2010). 3D architecture of a complex transcurrent rift system: The example of the Bay of Biscay-western Pyrenees. *Tectonophysics*, *489*(1–4), 210–226. <https://doi.org/10.1016/j.tecto.2010.04.023>
- Karner, G. D., & Watts, A. B. (1983). Gravity anomalies and flexure of the lithosphere at mountain ranges. *Journal of Geophysical Research*, *88*(B12), 10,449–10,477. <https://doi.org/10.1029/JB088iB12p10449>
- Kley, J., Monaldi, C. R., & Salfity, J. A. (1999). Along-strike segmentation of the Andean foreland: Causes and consequences. *Tectonophysics*, *301*(1–2), 75–94. [https://doi.org/10.1016/S0040-1951\(98\)90223-2](https://doi.org/10.1016/S0040-1951(98)90223-2)
- Lagabrielle, Y., & Bodinier, J.-L. (2008). Submarine reworking of exhumed subcontinental mantle rocks: Field evidence from the Lherz peridotites, French Pyrenees. *Terra Nova*, *20*(1), 11–21. <https://doi.org/10.1111/j.1365-3121.2007.00781.x>
- Larrasoána, J. C., Parés, J. M., Millán, H., del Valle, J., & Pueyo, E. L. (2003). Paleomagnetic, structural, and stratigraphic constraints on transverse fault kinematics during basin inversion: The Pamplona Fault (Pyrenees, north Spain). *Tectonics*, *22*(6), 1071. <https://doi.org/10.1029/2002TC001446>
- Lin, A. T., & Watts, A. B. (2002). Origin of the West Taiwan basin by orogenic loading and flexure of a rifted continental margin. *Journal of Geophysical Research*, *107*(B9), 2185. <https://doi.org/10.1029/2001JB000669>
- Lucas, C. (1985). Le grès rouge du versant nord des Pyrénées: Essai sur la géodynamique de dépôts continentaux du permien et du trias. Université de Toulouse.
- Lyon-Caen, H., & Molnar, P. (1983). Constraints on the structure of the Himalaya from an analysis of gravity anomalies and a flexural model of the lithosphere. *Journal of Geophysical Research*, *88*(B10), 8171–8191. <https://doi.org/10.1029/JB088iB10p08171>
- Lyon-Caen, H., & Molnar, P. (1985). Gravity anomalies, flexure of the Indian platen and the structure, support and evolution of the Himalayan and Ganga basin. *Tectonics*, *4*(6), 513–538. <https://doi.org/10.1029/TC004i006p00513>
- Masini, E., Manatschal, G., Tugend, J., Mohn, G., & Flament, J.-M. (2014). The tectono-sedimentary evolution of a hyper-extended rift basin: The example of the Arzacq–Mauléon rift system (western Pyrenees, SW France). *International Journal of Earth Sciences*, *103*(6), 1569–1596. <https://doi.org/10.1007/s00531-014-1023-8>
- Mauffret, A., Durand De Grossouvre, B., Tadeu Dos Reis, A., Gorini, C., & Nercessian, A. (2001). Structural geometry in the eastern Pyrenees and Western Gulf of Lion (western Mediterranean). *Journal of Structural Geology*, *23*(11), 1701–1726. [https://doi.org/10.1016/S0191-8141\(01\)00025-6](https://doi.org/10.1016/S0191-8141(01)00025-6)
- McKenzie, D. (1978). Some remarks on the development of sedimentary basins. *Earth and Planetary Science Letters*, *40*(1), 25–32. [https://doi.org/10.1016/0012-821X\(78\)90071-7](https://doi.org/10.1016/0012-821X(78)90071-7)
- Michon, L., & Merle, O. (2001). The formation of the west European rift: A new model exemplified by the massif central area. *Bulletin de la Société Géologique de France*, *172*(2), 213–221. <https://doi.org/10.2113/172.2.213>
- Molnar, P., & Lyon-Caen, H. (1988). Some simple physical aspects of the support, structure, and evolution of mountain belts. *Geological Society of America Special Papers*, *218*, 179–208. <https://doi.org/10.1130/SPE218-p179>
- Mouthereau, F., Filleaudeau, P., Vacherat, A., Pik, R., Lacombe, O., Fellin, M. G., ... Masini, E. (2014). Placing limits to shortening evolution in the Pyrenees: Role of margin architecture and implications for the Iberia/Europe convergence. *Tectonics*, *33*, 2283–2314. <https://doi.org/10.1002/2014TC003663>
- Muñoz, J. A. (1992). Evolution of a continental collision belt: ECORS-Pyrenees crustal balanced cross-section. In *Thrust Tectonics* (pp. 235–246). Dordrecht: Springer. https://doi.org/10.1007/978-94-011-3066-0_21
- Naylor, M., & Sinclair, H. D. (2008). Pro- vs. retro-foreland basins. *Basin Research*, *20*(3), 285–303. <https://doi.org/10.1111/j.1365-2117.2008.00366.x>
- Olivet, J. (1996). La cinématique de la plaque ibérique. *Bulletin des Centres de Recherches Exploration-Production Elf-Aquitaine*, *20*(1), 131–195.
- Olsen, P. E. (1997). Stratigraphic record of the early Mesozoic breakup of Pangea in the Laurasia-Gondwana rift system. *Annual Review of Earth and Planetary Sciences*, *25*(1), 337–401. <https://doi.org/10.1146/annurev.earth.25.1.337>
- Pedreira, D., Pulgar, J. A., Gallart, J., & Díaz, J. (2003). Seismic evidence of Alpine crustal thickening and wedging from the western Pyrenees to the Cantabrian Mountains (north Iberia). *Journal of Geophysical Research*, *108*(B4), 2204. <https://doi.org/10.1029/2001JB001667>
- Pedreira, D., Pulgar, J. a., Gallart, J., & Torné, M. (2007). Three-dimensional gravity and magnetic modeling of crustal indentation and wedging in the western Pyrenees-Cantabrian Mountains. *Journal of Geophysical Research*, *112*, B12405. <https://doi.org/10.1029/2007JB005021>
- Puigdefàbregas, C., & Souquet, P. (1986). Tecto-sedimentary cycles and depositional sequences of the Mesozoic and Tertiary from the Pyrenees. *Tectonophysics*, *129*(1–4), 173–203. [https://doi.org/10.1016/0040-1951\(86\)90251-9](https://doi.org/10.1016/0040-1951(86)90251-9)
- Rahl, J. M., Haines, S. H., & van der Pluijm, B. A. (2011). Links between orogenic wedge deformation and erosional exhumation: Evidence from illite age analysis of fault rock and detrital thermochronology of syn-tectonic conglomerates in the Spanish Pyrenees. *Earth and Planetary Science Letters*, *307*(1–2), 180–190. <https://doi.org/10.1016/j.epsl.2011.04.036>
- Roca, E., Muñoz, J. A., Ferrer, O., & Ellouz, N. (2011). The role of the Bay of Biscay Mesozoic extensional structure in the configuration of the Pyrenean orogen: Constraints from the MARCONI deep seismic reflection survey. *Tectonics*, *30*, TC2001. <https://doi.org/10.1029/2010TC002735>
- Rougier, G., Ford, M., Christophoul, F., & Bader, A.-G. (2016). Stratigraphic and tectonic studies in the central Aquitaine Basin, northern Pyrenees: Constraints on the subsidence and deformation history of a retro-foreland basin. *Comptes Rendus Geoscience*, *348*(3–4), 224–235. <https://doi.org/10.1016/j.crte.2015.12.005>
- Roure, F., Choukroune, P., Berastegui, X., Muñoz, J. A., Villien, A., Matheron, P., ... Deramond, J. (1989). Ecos deep seismic data and balanced cross sections: Geometric constraints on the evolution of the Pyrenees. *Tectonics*, *8*(1), 41–50. <https://doi.org/10.1029/TC008i001p00041>

- Royden, L. H., & Karner, G. D. (1984). Flexure of the continental lithosphere beneath Apennine and Carpathian foredeep basins. *Nature*, *309*(10), 19–21.
- Serranne, M. (1999). The Gulf of Lion continental margin (NW Mediterranean) revisited by IBS: An overview. *Geological Society, London, Special Publications*, *156*(1), 15–36. <https://doi.org/10.1144/gsl.sp.1999.156.01.03>
- Serrano, O., Delmas, J., Hanot, F., Vially, R., Herbin, J.-P., Houel, P., & Tourlière, B. (2006). Le bassin d'Aquitaine: valorisation des données sismiques, cartographie structurale et potentiel pétrolier (BRGM Ed).
- Serrano, O., Guillocheau, F., & Leroy, E. (2001). Évolution du bassin compressif Nord-Pyrénéen au Paléogène (bassin de l'Adour) : contraintes stratigraphiques. *Comptes Rendus de l'Académie des Sciences - Series IIA - Earth and Planetary Science*, *332*(1), 37–44. [https://doi.org/10.1016/S1251-8050\(00\)01487-7](https://doi.org/10.1016/S1251-8050(00)01487-7)
- Sibuet, J.-C., Srivastava, S. P., & Spakman, W. (2004). Pyrenean orogeny and plate kinematics. *Journal of Geophysical Research*, *109*, B08104. <https://doi.org/10.1029/2003JB002514>
- Sinclair, H. D., Gibson, M., Naylor, M., & Morris, R. G. (2005). Asymmetric growth of the Pyrenees revealed through measurement and modeling of orogenic fluxes. *American Journal of Science*, *305*(5), 369–406. <https://doi.org/10.2475/ajs.305.5.369>
- Souquet, P., Debroas, E.-J., Boirie, J.-M., Pons, P., Fixari, G., Roux, J.-C., ... Peybernès, B. (1985). Le groupe du flysch noir (Albo-Cénomani) dans les Pyrénées. *Bulletin Des Centres de Recherche Exploration-Production Elf-Aquitaine*, *9*(1), 183–252.
- Stewart, J., & Watts, A. B. (1997). Gravity anomalies and spatial variations of flexural rigidity at mountain ranges. *Journal of Geophysical Research*, *102*(B3), 5327–5352. <https://doi.org/10.1029/96JB03664>
- Stockmal, G. S., & Beaumont, C. (1987). Geodynamic models of convergent margin tectonics: the southern Canadian Cordillera and the Swiss Alps. *Sedimentary Basins and Basin-Forming Mechanisms*, *12*(40086), 393–411.
- Talwani, M., Worzel, J. L., & Landisman, M. (1959). Rapid gravity computations for two-dimensional bodies with application to the Mendocino submarine fracture zone. *Journal of Geophysical Research*, *64*(1), 49–59. <https://doi.org/10.1029/JZ064i001p00049>
- Teixell, A. (1998). Crustal structure and orogenic material budget in the west central Pyrenees. *Tectonics*, *17*(3), 395–406. <https://doi.org/10.1029/98TC00561>
- Teixell, A., Labaume, P., & Lagabrielle, Y. (2016). The crustal evolution of the west-central Pyrenees revisited: Inferences from a new kinematic scenario. *Comptes Rendus Geoscience*, *348*(3-4), 257–267. <https://doi.org/10.1016/j.crte.2015.10.010>
- The International Gravimetric Bureau (2012). *IAG geodesist's handbook, 2012*, *Journal of Geodesy* (Vol. 86). Springer.
- Torné, M., De Cabissole, B., Bayer, R., Casas, A., Daignières, M., & Rivero, A. (1989). Gravity constraints on the deep structure of the Pyrenean belt along the ECORS profile. *Tectonophysics*, *165*(1–4), 105–116. [https://doi.org/10.1016/0040-1951\(89\)90039-5](https://doi.org/10.1016/0040-1951(89)90039-5)
- Tugend, J., Manatschal, G., & Kusznir, N. J. (2015). Spatial and temporal evolution of hyperextended rift systems: Implication for the nature, kinematics, and timing of the Iberian-European plate boundary. *Geology*, *43*(1), 15–18. <https://doi.org/10.1130/G36072.1>
- Tugend, J., Manatschal, G., Kusznir, N. J., Masini, E., Mohn, G., & Thionon, I. (2014). Formation and deformation of hyperextended rift systems: Insights from rift domain mapping in the Bay of Biscay-Pyrenees. *Tectonics*, *33*, 1239–1276. <https://doi.org/10.1002/2014TC003529>
- Turcotte, D. L., & Schubert, G. (2002). In Camb (Ed.), *Geodynamics* (2nd ed.). Cambridge, UK: Cambridge University Press.
- Vacher, P., & Souriau, A. (2001). A three-dimensional model of the Pyrenean deep structure based on gravity modelling, seismic images and petrological constraints. *Geophysical Journal International*, *145*(2), 460–470. <https://doi.org/10.1046/j.0956-540x.2001.01393.x>
- Velasque, P. C., Ducasse, L., Muller, J., & Scholten, R. (1989). The influence of inherited extensional structures on the tectonic evolution of an intracratonic chain: The example of the western Pyrenees. *Tectonophysics*, *162*(3-4), 243–264. [https://doi.org/10.1016/0040-1951\(89\)90247-3](https://doi.org/10.1016/0040-1951(89)90247-3)
- Vergés, J., Millan, H., Roca, E., Muñoz, J. A., Marzo, M., Cirés, J., ... Cites, J. (1995). Eastern Pyrenees and related foreland basins: Pre-, syn- and post-collisional crustal-scale cross-sections. *Marine and Petroleum Geology*, *12*(8), 893–915.
- Vielzeuf, D., & Kornprobst, J. (1984). Crustal splitting and the emplacement of Pyrenean Iherzolites and granulites. *Earth and Planetary Science Letters*, *67*(1), 87–96. [https://doi.org/10.1016/0012-821X\(84\)90041-4](https://doi.org/10.1016/0012-821X(84)90041-4)
- Wang, Y., Chevrot, S., Monteiller, V., Komatitsch, D., Mouthereau, F., Manatschal, G., ... Martin, R. (2016). The deep roots of the western Pyrenees revealed by full waveform inversion of teleseismic P waves. *Geology*, *44*(6), 475–478. <https://doi.org/10.1130/G37812.1>
- Waschbusch, P. J., & Royden, L. H. (1992). Episodicity in foredeep basins. *Geology*, *20*(10), 915–918. [https://doi.org/10.1130/0091-7613\(1992\)020%3C0915:EIFB%3E2.3.CO;2](https://doi.org/10.1130/0091-7613(1992)020%3C0915:EIFB%3E2.3.CO;2)
- Watts, A. B. (1992). The effective elastic thickness of the lithosphere and the evolution of foreland basins. *Basin Research*, *4*(3–4), 169–178. <https://doi.org/10.1111/j.1365-2117.1992.tb00043.x>
- Watts, A. B. (2001). *Isostasy and flexure of the lithosphere*. Cambridge, UK: Cambridge University Press.
- Wessel, P., & Smith, W. H. F. (1991). Free software heps map and display data. *Eos, Transactions American Geophysical Union*, *72*(41), 441–448. <https://doi.org/10.1029/90EO00319>
- Willett, S. D., Chapman, D. S., & Neugebauer, H. J. (1984). Mechanical response of the continental lithosphere to surface loading: Effect of thermal regimes. *Annales Geophysicae*, *2*(6), 679–688.
- Zoetemeijer, R., Desegaulx, P., Cloetingh, S., Roure, F., & Moretti, I. (1990). Lithospheric dynamics and tectonic-stratigraphic evolution of the Ebro Basin. *Journal of Geophysical Research*, *95*(B3), 2701–2711. <https://doi.org/10.1029/JB095iB03p02701>